Pergamon

PII: S0306-4522(97)00530-7

Neuroscience Vol. 84, No. 2, pp. 377–402, 1998
Copyright © 1998 IBRO. Published by Elsevier Science Ltd
Printed in Great Britain. All rights reserved
0306–4522/98 $19.00+0.00

INHIBITORY CONTROL OF SOMATODENDRITIC INTERACTIONS UNDERLYING ACTION POTENTIALS IN NEOCORTICAL PYRAMIDAL NEURONS *IN VIVO*: AN INTRACELLULAR AND COMPUTATIONAL STUDY

D. PARÉ,* E. J. LANG and A. DESTEXHE

Département de Physiologie, Faculté de Médecine, Université Laval, Québec, Canada, G1K 7P4

Abstract—The effect of synaptic inputs on somatodendritic interactions during action potentials was investigated, in the cat, using *in vivo* intracellular recording and computational models of neocortical pyramidal cells. An array of 10 microelectrodes, each ending at a different cortical depth, was used to preferentially evoke synaptic inputs to different somatodendritic regions. Relative to action potentials evoked by current injection, spikes elicited by cortical microstimuli were reduced in amplitude and duration, with stimuli delivered at proximal (somatic) and distal (dendritic) levels evoking the largest and smallest decrements, respectively. When the inhibitory postsynaptic potential reversal was shifted to around -50 mV by recording with KCl pipettes, synaptically-evoked spikes were significantly less reduced than with potassium acetate or cesium acetate pipettes, suggesting that spike decrements are not only due to a shunt, but also to voltage-dependent effects. Computational models of neocortical pyramidal cells were built based on available data on the distribution of active currents and synaptic inputs in the soma and dendrites. The distribution of synapses activated by extracellular stimulation was estimated by matching the model to experimental recordings of postsynaptic potentials evoked at different depths. The model successfully reproduced the progressive spike amplitude reduction as a function of stimulation depth, as well as the effects of chloride and cesium. The model revealed that somatic spikes contain an important contribution from proximal dendritic sodium currents up to ≈ 100 μm and ≈ 300 μm from the soma under control and cesium conditions, respectively. Proximal inhibitory postsynaptic potentials can prevent this dendritic participation thus reducing the spike amplitude at the soma. The model suggests that the somatic spike amplitude and shape can be used as a "window" to infer the electrical participation of proximal dendrites.

Thus, our results suggest that inhibitory postsynaptic potentials can control the participation of proximal dendrites in somatic sodium spikes. © 1998 IBRO. Published by Elsevier Science Ltd.

Key words: multicompartment models, intrinsic electrophysiological properties, *in vivo* intracellular recordings, action potentials, dendritic integration.

By comparing the shape of antidromic, orthodromic and current-evoked action potentials (APs) in motoneurons, Coombs *et al.*[7] provided compelling evidence for the idea that APs are initiated at the initial segment (IS) and then invade the somatodendritic compartment. However, the applicability of this model to other cell types was questioned when the first intradendritic recordings revealed that dendrites can sustain active electrogenesis.[33,34,63]

In neocortical and hippocampal pyramidal neurons for instance, intracellular recordings revealed that dendritic spikes can be elicited by synaptic inputs[5,9,30,52] and that they can amplify synaptic inputs electrotonically distant from the soma to initiate APs.[5] Moreover, the proximal apical dendrites of pyramidal neurons were found to contain voltage-gated Ca^{2+} and Na^{+} conductances capable of generating current densities similar to those observed at the soma.[25,38,59] Consistent with this, imaging techniques revealed that synaptic activation and membrane depolarization can elicit significant increases in intracellular Ca^{2+} concentration through the opening of dendritic voltage-gated channels.[25a,39,40,42,54,67]

Nevertheless, dual intracellular recordings from the dendrites and soma or initial axonal segment of pyramidal cells from newborn rats showed that current-evoked and orthodromic APs are first initiated in the axon and then invade the apical dendrite through the activation of somatic and dendritic Na^{+} conductances.[59] In a computational analysis of this phenomenon, Mainen *et al.*[41] proposed that the failure of dendritic Na^{+} channels to initiate APs is due to the fast inactivation of Na^{+} channels compared to the membrane time constant and to source–load interactions opposing membrane charging from the dendrites to the soma.

*To whom correspondence should be addressed.

Abbreviations: ABC, avidin–biotin–peroxidase complex; AMPA, α-amino-3-hydroxy-5-methyl-4-isoxalone propionic acid; APs, action potentials; EEG, electroencephalogram; EPSP, excitatory postsynaptic potential; IPSP, inhibitory postsynaptic potential; IS, initial segment; NMDA, *N*-methyl-D-aspartate; PBS, phosphate-buffered saline; PSP, postsynaptic potential.

The retrograde invasion of dendrites by APs could have a profound impact on pyramidal neurons. Indeed, backpropagating spikes might lead to Ca^{2+} entry through the activation of voltage-gated Ca^{2+} channels and/or by temporarily removing the Mg^{2+} block of *N*-methyl-D-aspartate (NMDA) channels.[43] Considering the impact of intracellular Ca^{2+} levels on various forms of synaptic plasticity,[3] it is important to determine how inhibitory synaptic inputs affect the dendritic participation in somatic APs under *in vivo* conditions where the cortical circuitry is intact. To this end, we performed intracellular recordings of morphologically-identified neocortical pyramidal neurons in anaesthetized cats and compared APs evoked by synaptic inputs, antidromic invasion, or direct current injection. This data was then used to constrain a biophysical model of a pyramidal neuron integrating available information about the distribution of synaptic inputs and Na^+ current densities.

EXPERIMENTAL PROCEDURES

Preparation of the animals and recording methods

Experiments were performed in adult cats (Service des animaux de laboratoire, University Laval, Québec, Canada) deeply anaesthetized with sodium pentobarbital (Somnotol, 40 mg/kg, i.p.), paralysed with gallamine triethiodide (Flaxedil, i.v.) and artificially ventilated. The end-tidal CO_2 concentration was kept at $3.7 \pm 0.2\%$ and the body temperature was maintained at 37–38°C with a heating pad. To insure that the animals were anaesthetized for the entire duration of the experiments, the electroencephalogram (EEG) (recorded from the pericruciate region) was continuously monitored and supplementary doses of pentobarbital (5–7 mg/kg, i.v.) were administered to maintain a synchronized EEG pattern. Furthermore, a local anaesthetic (Lidocaine, 2%) was injected into the tissues to be incised. The stability of the recordings was ensured by performing a cisternal drainage, a bilateral pneumothorax, suspending the hips, and covering the cortex with a warm agar solution (3.5% in 0.9% saline).

Intracellular recordings of cortical neurons were performed with micropipettes (tip diameter ≈ 0.4 μm; 35–60 MΩ) filled with one of the following solutions: K-acetate (KAc; 4 M), Cs-acetate (CsAc; 3.0 M), KCl (3.0 M), or CsCl (3.0 M). In many experiments, Neurobiotin (Vector Labs; 1.5%) was added to the solution to morphologically identify the recorded cells. A high-impedance amplifier with active bridge circuitry was used to record the membrane potential (V_m) and for intracellular current injection. Measurements were taken after stabilization of the impalement. Recordings usually lasted for 30 min to two hours. An array of 10 stimulating microelectrodes was inserted obliquely in cortical areas 5–7 (Fig. 1A) so that the inter-tip spacing was approximately 150 μm in the dorsoventral axis (Fig. 1B). Cortical neurons were recorded 1–2 mm from the electrode array. Electrical stimuli consisted of 50–100 μs pulses (100–750 μA).

Signals were observed on a digital oscilloscope, printed on a chart recorder, digitized at 12 kHz and stored on tape. Analyses were performed off-line with the computer program IGOR (Wavemetrics, Oregon) and homemade software. The input resistance (R_{in}) of recorded neurons prior to and at the peak of cortically-evoked inhibitory postsynaptic potential (IPSPs) was estimated by calculation of the slope resistance (the reciprocal of the slope conductance[26]). Here, the change in voltage from the resting V_m was plotted against the d.c. current level, and the slope of the fitted line was used to estimate the R_{in} of the cell. When comparing the reversal potential or R_{in} drop related to IPSPs evoked by cortical stimuli applied at different depths, the same stimulation intensity was used at all stimulation sites. The stimulation intensity was first adjusted with the most superficial electrodes. It was increased gradually to just below spike threshold at -60 mV. Thereafter, the same stimulation intensity was used for deeper electrodes.

Histological identification of the recorded cells and stimulation sites

At the end of the experiments, the animals were perfused with 500 ml of a cold saline solution (0.9%) followed by 1 l of a fixative containing 2% paraformaldehyde and 1% glutaraldehyde in 0.1 M phosphate-buffered saline (PBS, pH 7.4). A block of cortex containing the recorded cells was then dissected and stored in PBS at 4°C until it was sectioned on a vibrating microtome (at 80 μm). Sections were incubated in an avidin–biotin–peroxidase complex solution (ABC Elite kit, Vector Labs) and processed to reveal the intracellular peroxidase staining.[23] In addition, selected sections were counterstained with Thionin to verify the positions of the stimulating electrodes. Tissue shrinkage induced by fixation was estimated at $\approx 15\%$.

Computational models

Morphology. Simulations of a neocortical layer V pyramidal cell were based on a cellular reconstruction provided by R. Douglas and K. Martin. The cell was recorded intracellularly in cat visual cortex,[13] stained with horseradish peroxidase and reconstructed using a computerized tracing system. Simulations were performed using NEURON,[21] which can read and convert geometry files from several tracing systems. The cell was digitized into 440 compartments and constrained with a maximal compartment length of 50 μm. Digitization using a maximal compartment length of 10 μm had no detectable consequences for the results presented here.

Layer V neocortical pyramidal cells have a high density of dendritic spines, in the range of 8000–14,000 spines/cell in rat visual cortex.[32] This represents about 25–45% of the total cell surface.[8,46] Thus, in the model, the dendritic surface was corrected by assuming a uniform spine density that increased the dendritic surface by 45% ($\approx 30\%$ of the cell surface). Surface correction was made by rescaling the size of each compartment or by rescaling the values of the capacitance and conductances in dendrites by a factor of 1.45. Both methods gave similar results.

An axon was modelled on the basis of serial electron microscopic measurements of neocortical pyramidal cells,[15] as described previously.[41] The axon consisted of a 10 μm hillock, a 15 μm unmyelinated IS and 504 μm of axon proper. The axon hillock had 10 compartments arranged in a conical form, tapering from 4.3 μm at the soma level to 1 μm at the level of the axon IS. The IS consisted of 10 compartments (1 μm diameter). The axon proper was divided into five myelinated compartments of 100 μm, interleaved with nodes of Ranvier (length of 1 μm) having a higher density of Na^+ channels (see details in Ref. 41). The axon was also simulated using a single equivalent cylinder for each compartment (hillock and IS only), and only minimal differences were found with respect to the detailed model.

Passive parameters. In order to obtain a correct time constant and R_{in}, passive parameters were estimated by fitting the model to a voltage trace from a layer V cortical pyramidal cell recorded in the present series of experiments. The fit was performed using a simplex fitting algorithm.[50] For a given cellular geometry and assuming uniform passive properties (leak conductance, g_{leak} and reversal potential,

E_{leak}, specific capacitance (C_m) and specific intracellular resistivity (R_i) in the soma and dendrites, multiple solutions were possible. Thus, the fit was further constrained by setting the capacitance to C_m=1 μF/cm^2, a typical value for neuronal membranes. The fitting procedure then converged to a unique set of passive parameters from different initial conditions.

Active membrane properties. Active currents were inserted into the soma, dendrites and axon with different densities in accordance with available biophysical evidence. In light of patch-clamp data showing that the soma and dendrites of neocortical and hippocampal pyramidal cells have similar Na^+ channel densities,[25,38,59] the Na^+ conductance was set to 70 pS/μm^2 (range tested 20–100) in dendritic and somatic compartments. This value corresponds to the estimated value for Na^+ channel densities in adult pyramidal neurons of the hippocampus.[38]

The density of Na^+ channels in the IS is controversial as various estimates have been obtained depending on the cell types and techniques used.[1,5a,47a,62a] Binding studies show an increased Na^+ channel density in the IS.[1,62a] On the other hand, a patch-clamp study on subicular neurons has concluded that the Na^+ channel density in the IS is similar to that of the soma.[5a] Yet, models of spike initiation in neocortical pyramidal cells predict an increased Na^+ channel density in the IS[1a,41] or the axon.[51] In particular, it was demonstrated that restricting high Na^+ channel densities to the axon (with low densities in IS), or high densities in both axon and IS, gave very similar results with respect to spike backpropagation.[51] In the present model, a Na^+ conductance of 40,000 pS/μm^2 (tested range, 20,000–50,000 pS/μm^2) was chosen for the IS and nodes of Ranvier.[5a] This value lies within the range of Na^+ channel density estimated in the axon in binding and immunohistochemical studies[2] but is higher than that found in the IS of subicular neurons with electrophysiological techniques.[5a] This high density was required to reproduce the overshooting somatic APs observed in most *in vivo* intracellular recordings while being consistent with Na^+ conductance densities of 70 pS/μm^2 in the soma and dendrites. The Na^+ channel density of the internodal segments was set at the same value as the soma and dendrites.

The delayed-rectifier K^+ conductance (Kd) was inserted into dendrites and soma with a density of 100 pS/μm^2 (tested range, 20–300 pS/μm^2). In the axon IS and nodes of Ranvier, a density of 1000 pS/μm^2 was used. A non-inactivating K^+ conductance (M) was also included in the soma and dendrites with a density of 5 pS/μm^2. This value was required to reproduce the repetitive firing behaviour of neocortical pyramidal neurons observed *in vivo*.

Some simulations were carried out in the presence of high-threshold Ca^{2+} currents (I_{CaH}) and Ca^{2+}-dependent K^+ currents ($I_{K[Ca]}$). In this case, the Ca^{2+} conductance density was 30 pS/μm^2 in the soma and first 50 μm of the proximal dendrites, and 15 pS/μm^2 in the rest of the dendritic tree, according to the densities estimated in hippocampal pyramidal cells by patch-clamp recordings.[38] A voltage-independent Ca^{2+}-dependent K^+ conductance was also inserted with a uniform density of 10 pS/μm^2 in soma and dendrites.

The kinetics of the Na^+ current (I_{Na}), I_{CaH}, I_{Kd}, $IK_{[Ca]}$ and I_M were described by Hodgkin and Huxley type equations[22] and were solved using NEURON.[21] Kinetics for I_{Na} and I_{Kd} were taken from models of hippocampal pyramidal cells,[60] with reversal potentials of +50 mV and −90 mV, respectively. The kinetics of I_M and I_{CaH} were taken from previous models of neocortical pyramidal cells.[17,53] Intracellular Ca^{2+} and $IK_{[Ca]}$ were modelled as in Ref. 10. All simulations corresponded to a temperature of 36°C (temperature factor for time constants was Q_{10}=3). The kinetic equations used to model intrinsic currents and Ca^{2+} dynamics are listed in the Appendix.

Synaptic inputs. In our model, three parameters controlled synaptic inputs: (i) the relative density of excitatory and inhibitory synapses in different regions of the cell, (ii) the fraction of these synapses activated by a given stimulus, and (iii) the kinetics of the currents mediated by the different types of receptors involved.

The relative density of glutamatergic and GABAergic synapses in each region of the cell was constrained by morphological data (reviewed in Ref. 8). Electron microscopic observations of neocortical pyramidal cells have established that the soma, axon hillock and IS exclusively form symmetric synaptic contacts[29,49] that are most likely GABAergic.[8,62] Quantitative studies have revealed that the density of symmetric synapses on the soma of deep pyramidal cells is 10.6 ± 3.7/100 μm^2 whereas the IS forms 20–24 symmetric synapses.[14,15] The latter yields a GABAergic synaptic density of ≈45/100 μm^2 on the modeled IS given that its surface area was 47.1 μm^2. A similar density was assumed for the axon hillock.

About 16% of the total number of synapses found on neocortical pyramidal cells are of the symmetric variety: 7% of these end on the soma and 93% in the dendrites.[8] Given that the modelled neuron had a soma surface of 1453 μm^2 and a dendritic surface of 52808 μm^2, this yields a ratio of ≈3:1 in favour of the soma. Thus, in our model, the relative densities of GABAergic synapses were 0.17 in the apical and basal dendrites, 0.6 in the soma, and 2.5 in the axon hillock and IS.

In neocortical pyramidal neurons, the vast majority of asymmetric synapses are found on dendritic spines.[62] Thus, in our model, excitatory synapses were exclusively located in the dendrites, with a uniform density, except for the most proximal dendritic segments (up to 30 μm from soma) that are devoid of spines[28,48] and mostly form symmetric synapses.[29]

To simulate synaptic responses of pyramidal cells observed in the present study, the model pyramidal cell was divided into three regions: (1) Proximal—basal dendrites, soma and initial 200 μm of the apical dendrite; (2) Middle—the next 500 μm of the apical dendrite; (3) Distal—the remainder of the apical dendrite. These regions are illustrated in Fig. 10A. Within these three regions, the fraction of synaptic currents activated by extracellular stimulation was estimated by comparing the model with experimental recordings of EPSP/IPSP sequences evoked at different depths. The R_{in} change, reversal potential, amplitude and time-to-peak of EPSP/IPSPs evoked by extracellular stimulation at different depths were used to constrain the values of synaptic conductance in the different regions of the cell. This procedure is detailed in the Results.

The kinetics of synaptic currents were modelled using two-state kinetic models of α-amino-3-hydroxy-5-methyl-4-isoxalone proprionic acid (AMPA), NMDA and $GABA_A$ receptors.[11] Other types of synaptic responses were not included because they were not required to account for the behaviour of the cells and because GABAergic and glutamatergic synapses account for the vast majority of synapses in the cerebral cortex.[8,62] Based on whole-cell recordings of hippocampal pyramidal and dentate gyrus cells,[19,47,64] kinetic models of $GABA_A$, NMDA and AMPA receptors were fitted to experimental data using a simplex procedure (see details in Ref. 12). The kinetic equations and parameters for synaptic currents are detailed in the appendix.

RESULTS

Database and morphological features of recorded neurons

Stable intracellular recordings were obtained from area 5–7 cortical neurons (Fig. 1A–C) that had

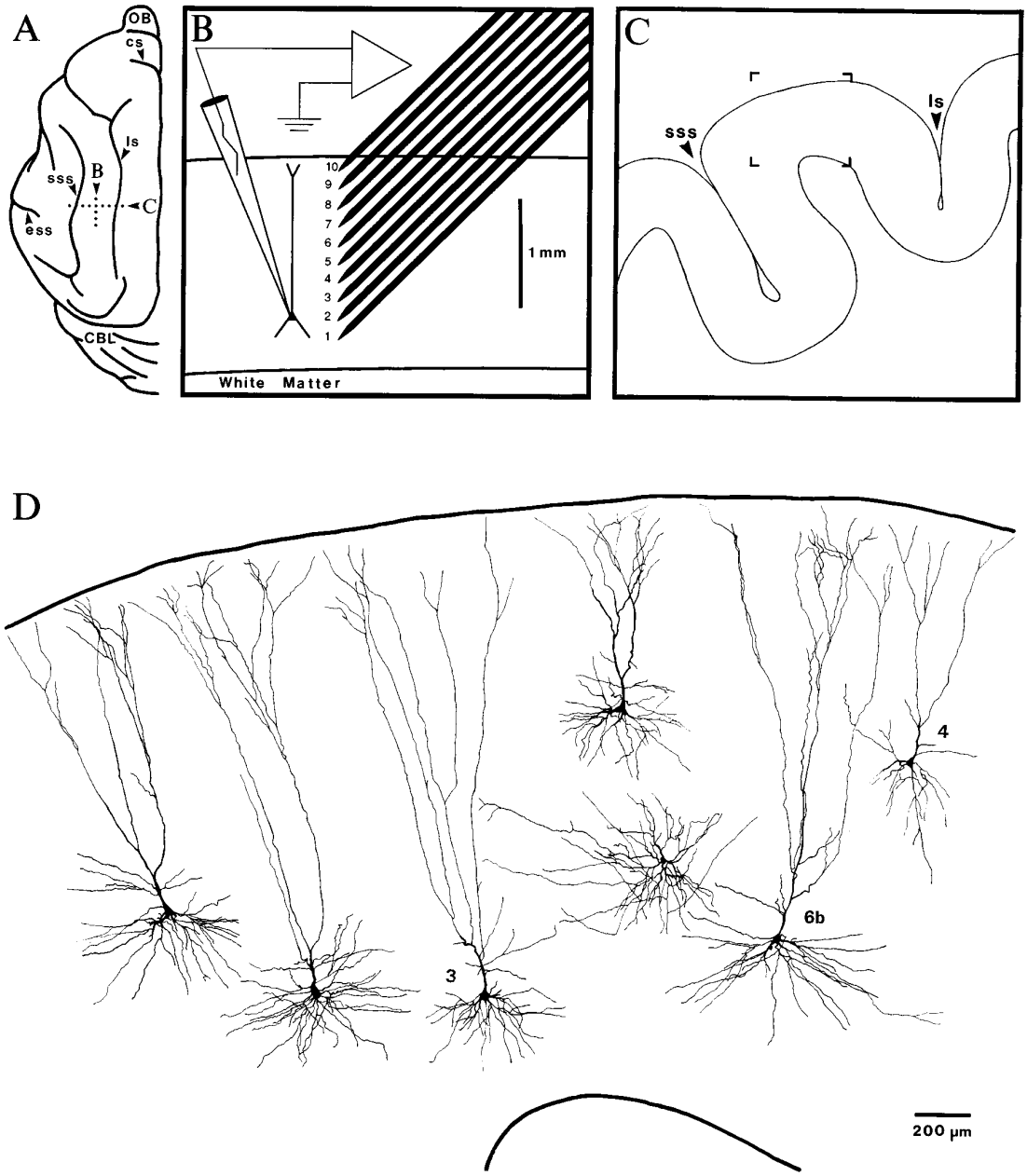

Fig. 1. Experimental paradigm and morphological identification of area 5–7 cortical neurons. (A) Dorsal view of the left hemisphere of a cat brain. Dotted lines labelled B or C indicate the plane of the sections shown in panels B and C, respectively. (B) Scheme of the experimental paradigm. Sagittal section through the suprasylvian gyrus with the array of 10 stimulating electrodes used to deliver electrical stimuli at various cortical depths. This scheme is not drawn to scale. The distance between the stimulating electrodes and the recording site was 1–2 mm. (C) Frontal section of the suprasylvian gyrus. Area enclosed in brackets is shown at a higher magnification in D. (D) Drawings of seven suprasylvian neurons filled with neurobiotin and partially reconstructed from three to five consecutive sections. The numbers indicate figures where the synaptic responses of the corresponding cells are depicted. The scale bar in D was adjusted for the tissue shrinkage that resulted from fixation (15–20%). cs, cruciate sulcus; CBL, cerebellum; ess, ectosylvian sulcus; ls, lateral sulcus; OB, olfactory bulb; sss, suprasylvian sulcus.

resting potentials $\geqslant -60$ mV and APs ranging between 55 and 80 mV (n=82). All but two of the morphologically-identified cells (n=42) were regular spiking[6,45] pyramidal neurons (Figs 1D, 2A–B) whose somata were located in the infragranular (n=24) or supragranular layers (n=16), 1 to 2 mm from the cortical stimulating electrode array (Fig. 1A–B).

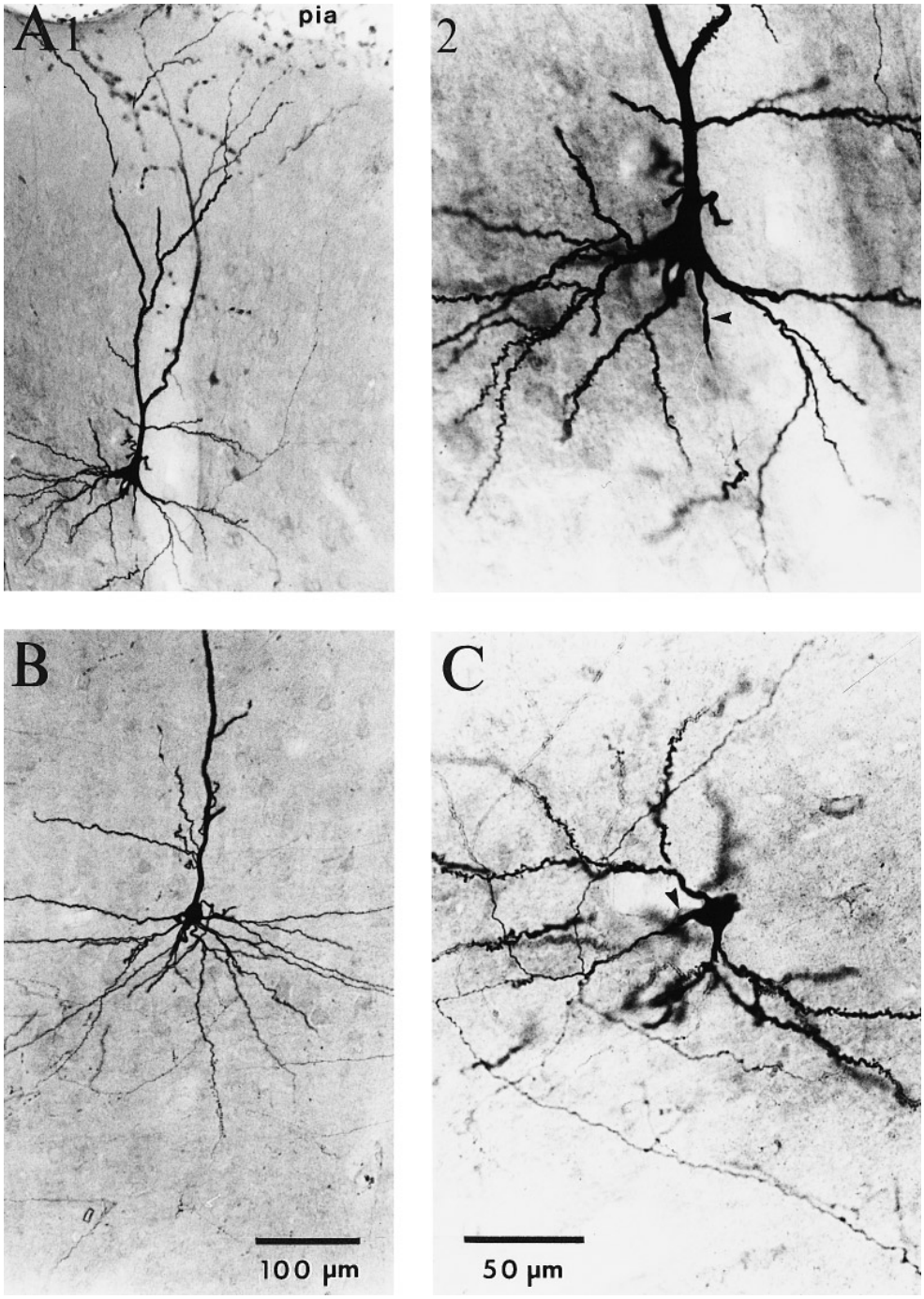

Fig. 2. Morphological features of suprasylvian neurons. (A) Photomicrographs of a superficial pyramidal neuron at low (A1) and high (A2) magnification. (B) Deep pyramidal neuron. (C) Photomontage of high-power photomicrographs showing a layer IV spiny stellate neuron. Arrowheads in A2 and C point to the IS of the axon, which usually arose from the soma. Scale bar in B also valid for A1. Scale bar in C also valid for A2.

Comparison between direct and orthodromic spikes in pyramidal cells under cesium acetate

In the course of experiments on the genesis of IPSPs, we fortuitously observed that the shape of APs generated by pyramidal neurons recorded with CsAc pipettes (n=16) varied markedly depending on whether they were triggered synaptically or by current injection. Figure 3 illustrates this phenomenon in a morphologically-identified layer V pyramidal neuron (labelled 3 in Fig. 1D). Upon steady depolarization to firing threshold, deep pyramidal cells generated broad APs (7–20 ms at the base, Fig. 3) that sometimes gave rise to a second, slower AP or to

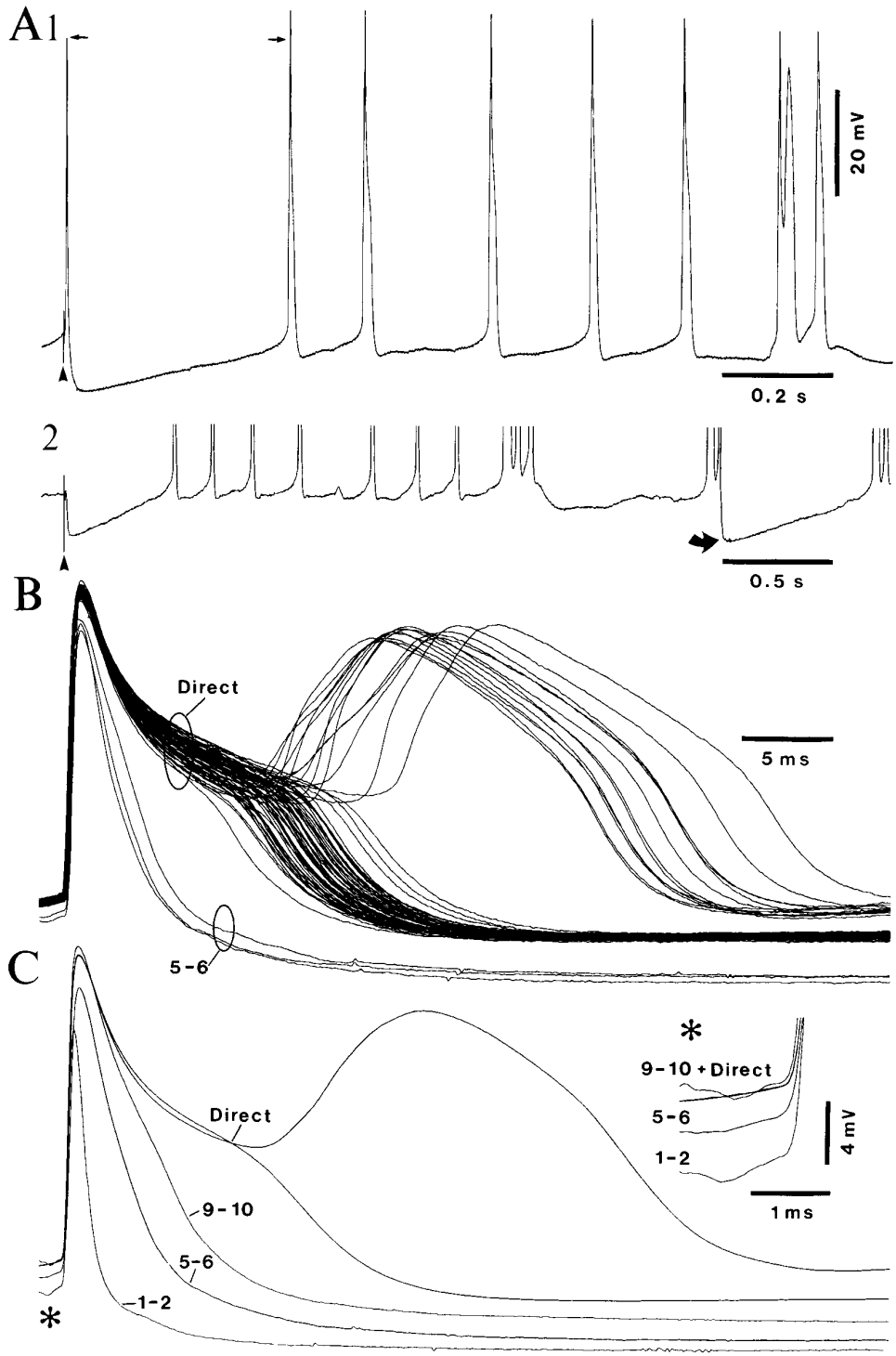

Fig. 3. Cortical stimuli applied in deep cortical layers are more effective in reducing the APs generated by layer V pyramidal neurons. Morphologically-identified layer V pyramidal neuron (labeled 3 in Fig. 1) recorded with a CsAc pipette. This cell was depolarized from rest (-64 mV) to -60 mV by steady current injection until it fired APs at frequencies ranging between 4 and 7 Hz. Cortical stimuli of constant intensity (0.2 mA for 0.1 ms at 0.2 Hz) were applied at different depths (1–2 $\approx$ 1400 μm; 5–6 $\approx$ 800 μm; 9–10 $\approx$ 200 μm). In A1, note that the spike elicited by a shock delivered through electrodes 5–6 (arrowhead) was decreased in amplitude (arrows) and duration compared to the spikes evoked by current injection. A2 shows a subthreshold response to the same stimulus (arrowhead) and a spontaneously occurring IPSP (curved arrow). Note the short duration of the spike preceding the spontaneous IPSP. In panel B, spikes evoked by current injection (Direct) and cortical stimuli 5–6 are superimposed. In C, averages of spikes evoked by current injection (Direct) and cortical stimuli delivered at different depths were superimposed. Although all stimulation sites reduced the amplitude and duration of APs, deep sites produced the largest decrements. The inset in C (asterisk) shows that the spike threshold was more hyperpolarized for spikes elicited by deep stimulation sites (1–2 and 5–6) than for those elicited by superficial stimuli (9–10) or current injection (Spont.).

prolonged depolarizing plateaus (0.5–5 s) crowned by an oscillation at 25–35 Hz (not shown).

In comparison to current-evoked spikes, orthodromic APs elicited by juxta-threshold cortical stimuli (Fig. 3A, arrowhead) or occurring in relation to spontaneous EEG events (not shown) were reduced in amplitude and duration. In deep pyramidal neurons, the magnitude of this reduction was related to the stimulation site with superficial (9–10, Fig. 3C) and deep (1–2, Fig. 3C) cortical stimuli, respectively, producing the smallest and largest decrements, whereas stimuli delivered to mid-cortical layers produced intermediate reductions (5–6, Fig. 3B–C). For instance, in the deep pyramidal cell of Fig. 3, current-evoked APs (Direct) averaged 62 mV in height and 16 ms in duration (measured at the base). In comparison to direct spikes, the voltage peak of orthodromic spikes evoked by 1–2, 5–6 and 9–10 was reduced by 15.5, 7.5 and 1.5 mV and their duration by 13.8, 10.2 and 7.3 ms, respectively. Here, it is important to note that by blocking I_{Kd} and some Ca^{2+}-dependent K^+ currents,[20,65] Cs^+ reduced the R_{in} drop normally occurring during the spike repolarization thus maximizing the dendritic depolarization caused by the somatic spike and allowing the soma to "see" more of the active dendritic events triggered by the somatic AP.

To quantify this phenomenon across our sample of deep pyramidal cells, these reductions were normalized to the amplitude and duration of current-evoked spikes. On average, 1–2 reduced the spike peak by $25.1 \pm 4.3\%$ and its duration by $87.9 \pm 3.4\%$ (mean ± S.E.M.) compared to $4.4 \pm 0.2\%$ and $30.8 \pm 9.1\%$ with 9–10. These differences were statistically significant (paired t-test, $P<0.01$). Intracortical stimuli could also terminate the prolonged plateau potentials occasionally observed under Cs^+ (not shown).

The same phenomena were observed in superficial pyramidal neurons (layers II–III) except that the stimulation sites producing the largest decrements were more superficial, in close correspondence with the soma position. For instance, the soma of the pyramidal cell shown in Fig. 4 (labelled 4 in Fig. 1D) was located at a depth of 0.66 mm. Maximal spike reductions were obtained by stimulating close to the soma level (6–7; Fig. 4). Deeper and shallower stimulation sites produced progressively smaller decrements (Fig. 4).

The above results suggested that the differential effectiveness of cortical stimuli applied at different depths in modifying the spike shape resulted from the activation of afferent fibres preferentially ending at corresponding cortical levels. To test this idea, we compared the electrophysiological features of IPSPs elicited by stimuli of equal intensities, but applied at various cortical depths. In four layer V pyramidal neurons analysed in detail, the IPSPs elicited by deep cortical shocks were larger in amplitude (12.4 ± 2.25 mV compared to 4.8 ± 1.89 mV), had a shorter peak-latency (23.4 ± 2.93 ms compared to 41.3 ± 5.33 ms), a more positive reversal potential (-73.8 ± 1.64 mV compared to -80.3 ± 1.75 mV) and were associated with larger decreases in R_{in} ($63 \pm 8.4\%$ compared to $27 \pm 5.1\%$) than those elicited by superficial cortical stimuli. These differences were statistically significant (paired t-test, $P<0.05$). Electrical stimuli applied to mid-cortical layers elicited IPSPs that displayed intermediate values. In addition, response latencies gradually increased from deep to superficial stimuli (1–2, 2.3 ± 0.68 ms; 3–4, 2.9 ± 0.71 ms; 5–6, 3.2 ± 0.78 ms; 7–8, 4.0 ± 0.93 ms; 9–10, 5.3 ± 1.25 ms; $n=6$).

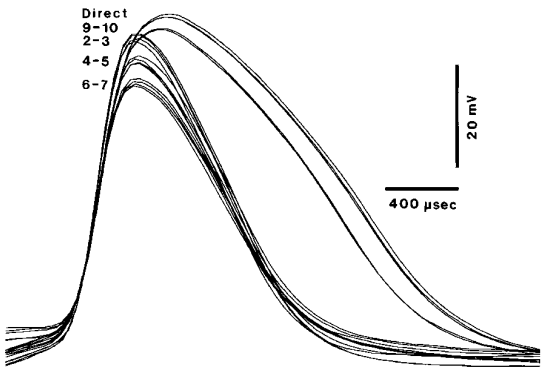

Fig. 4. Cortical stimuli applied in mid-cortical layers are the most effective in reducing the AP generated by layer III pyramidal cells. Morphologically-identified layer III pyramidal neuron (labeled 4 in Fig. 1) recorded with a CsAc-pipette. Spikes elicited by short depolarizing current pulses (direct) or by subthreshold cortical shocks applied during a juxtathreshold depolarizing current pulse are superimposed. Numbers indicate stimulation site (see Fig. 1B). Note that stimuli delivered through electrodes 6–7 were most effective in reducing the spike amplitude and duration.

Figure 5 illustrates this phenomenon in a representative deep pyramidal cell. In this neuron, the IPSP reversal measured at the IPSP peak shifted by approximately -7 mV from deep to superficial cortical stimuli and this shift was associated with a 48% reduction in the R_{in} drop measured at the IPSP peaks (Fig. 5C). As shown in Fig. 5D, these differences in the reversal potentials of IPSPs as a function of the stimulation site were relatively constant throughout the duration of the IPSPs with the exception of their initial phases that were contaminated by EPSPs. Note that performing this analysis in cells recorded with CsAc pipettes eliminated the complication related to the possible segregation of $GABA_A$ and $GABA_B$ receptors in different cellular compartments as Cs^+ blocks $GABA_B$ IPSPs.[16]

These results suggest that cortical stimuli delivered at different depths activate partially segregated sets of afferents that preferentially end at corresponding cortical depths, thus exerting maximal effects on different compartments of pyramidal neurons.

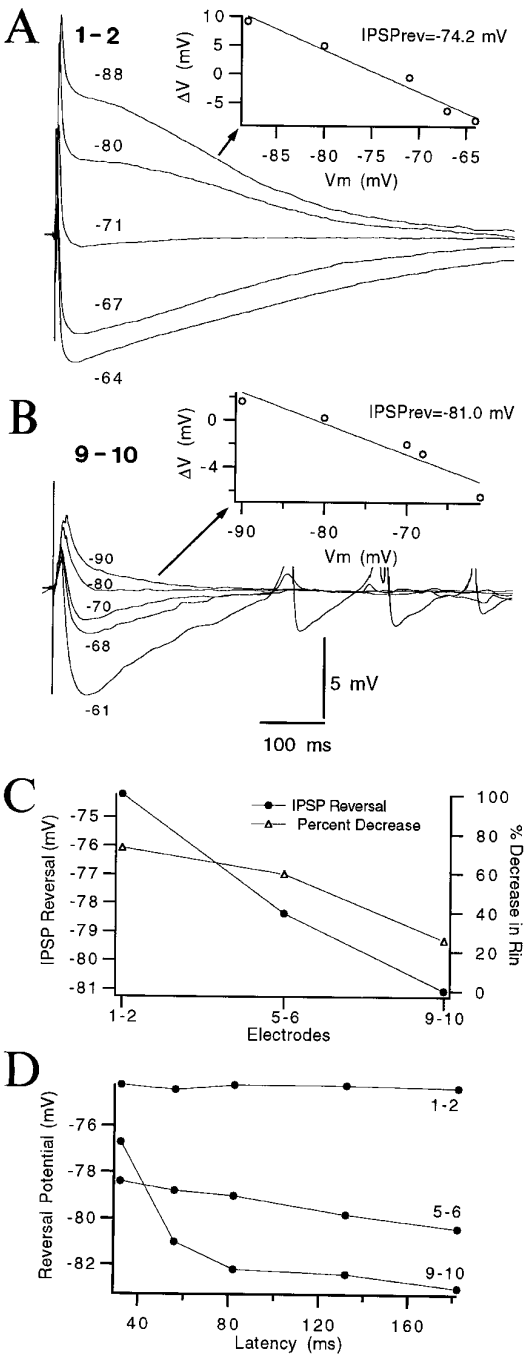

Fig. 5. Graded changes in cortically-evoked IPSPs as a function of stimulation depth. Same cell, stimulation sites and intensity as in Fig. 3. Panels A and B depict how IPSPs elicited by cortical stimuli delivered at different depths vary with V_m (as determined by current injection). Numbers adjacent to traces indicate V_m. Graphs on the right plot the IPSP amplitude (ΔV) as a function of V_m. In C, the IPSP reversal and associated percent decrease in R_{in} (measured at the IPSP peak, see Experimental Procedures) is plotted as a function of the cortical stimulation site. Note that the IPSP reversal potential shifted from -74 mV with deep stimulation sites (1–2) to -81 mV with superficial stimuli (9–10). This shift was parallelled by a progressive reduction in the R_{in} decrement produced by the IPSP. (D), Graph plotting the IPSP reversal potentials as a function of the interval between the cortical shocks and the IPSP measurements.

Influence of postsynaptic potentials on action potentials generated by pyramidal neurons under potassium acetate

In the experiments described above, the intracellular diffusion of Cs^+ probably modified the spike shape by blocking a variety of K^+ channels including I_{Kd} and some Ca^{2+}-dependent K^+ channels.[20,65] These actions of Cs^+ prolonged the spike duration by interfering with the spike repolarization thus allowing APs to activate inward conductances that are probably not activated to such an extent in normal circumstances.

To verify if cortically-evoked postsynaptic potentials (PSPs) could modify the spike shape under more physiological conditions, similar tests were performed in pyramidal cells recorded with KAc pipettes (n=29). At first, the intensity of the cortical stimuli was adjusted to just above the spike threshold from rest. Compared to APs elicited by short depolarizing current pulses (Fig. 6A1), orthodromic spikes were reduced in amplitude and duration (Fig. 6A2–3). As was observed with CsAc recordings, the magnitude of the amplitude decrement was a function of the cortical stimulation depth relative to the position of the recorded cells.

In deep pyramidal neurons, superficial and deep cortical stimuli produced the smallest and largest amplitude decrements, respectively. To quantify this phenomenon across our sample, these reductions were normalized to the amplitude of current-evoked spikes. On average, deep stimuli (1–2 or 3–4) reduced the spike peak by $22.8 \pm 3.14\%$ compared to $9.4 \pm 1.11\%$ for superficial stimuli (7–8 or 9–10; n=7). These differences were statistically significant (paired t-test, $P<0.01$). For example, in the layer V pyramidal cell of Fig. 6A, deep cortical stimuli reduced the spike peak by 19 mV whereas superficial stimuli only produced a 8 mV decrement. The reductions in spike duration were much smaller than observed in CsAc recordings, but generally paralleled the amplitude reductions. For instance, in the layer V pyramidal cell of Fig. 6A4, the spike duration (measured at the base) was 1.08 and 1.17 ms for 3–4 and 7–8 compared to 1.33 ms for the APs elicited by current injection. However, measurements of spike duration had limited significance because deep cortical stimuli often slowed the transition between the IS and somatodendritic components of the AP, as evidenced by the break in the rising phase of the spikes. Consequently, no further attempt was made to quantify these changes.

In comparison to APs elicited by intracellular current injection, spontaneous orthodromic APs generated by pyramidal neurons were also reduced in amplitude. The decrements in the amplitude of spontaneous spikes were variable (range 1–12 mV) but were observed in the vast majority of neurons (79%; n=29).

To insure that the differences between the shapes of direct and orthodromic spikes did not reflect

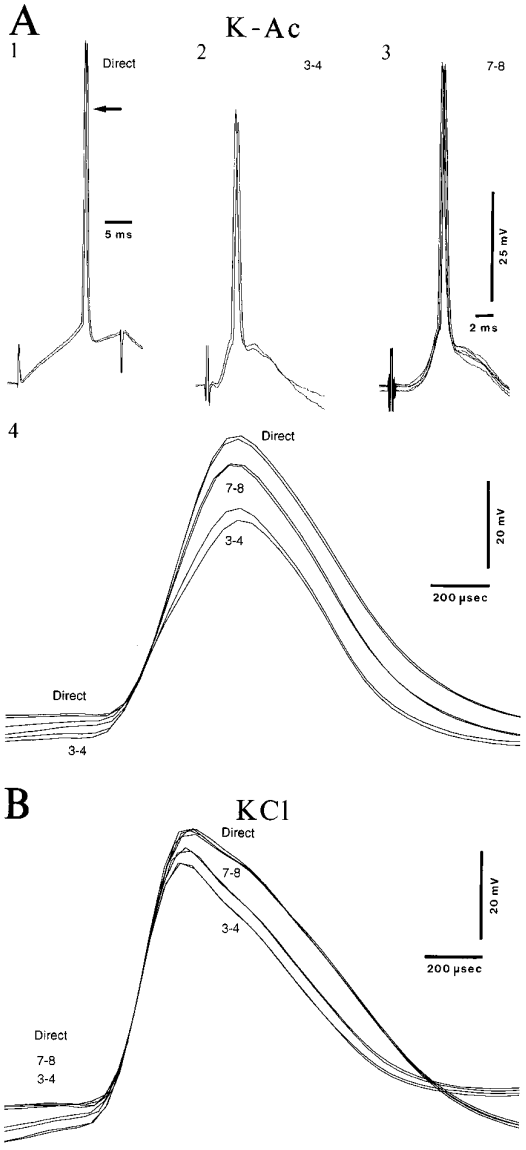

Fig. 6. Orthodromic spikes elicited from rest are reduced in amplitude and duration. Pyramidal neurons with somata located in the superficial part of layer V. (A) KAc-pipette. Spikes were evoked by depolarizing current pulses (0.7 nA, Direct, A1) from rest (−69 mV) or by juxtathreshold cortical shocks delivered at the level of the soma (A2) or distal apical dendrites (A3). Numbers in the upper right of panels A2–3 indicate stimulating electrodes (see Fig. 1B). A4 displays superimposed orthodromic and direct spikes with an expanded time base. (B) KCl-pipette. Superimposed direct (0.5 nA) and orthodromic spikes elicited from rest (−64 mV). The morphological features of this cell can be seen in Fig. 1 where it is labeled "6b". Numbers indicate stimulating electrodes (see Fig. 1B). The spike amplitude could not be reduced further by increasing the stimulation intensity. Note smaller spike reduction in the cell recorded with KCl.

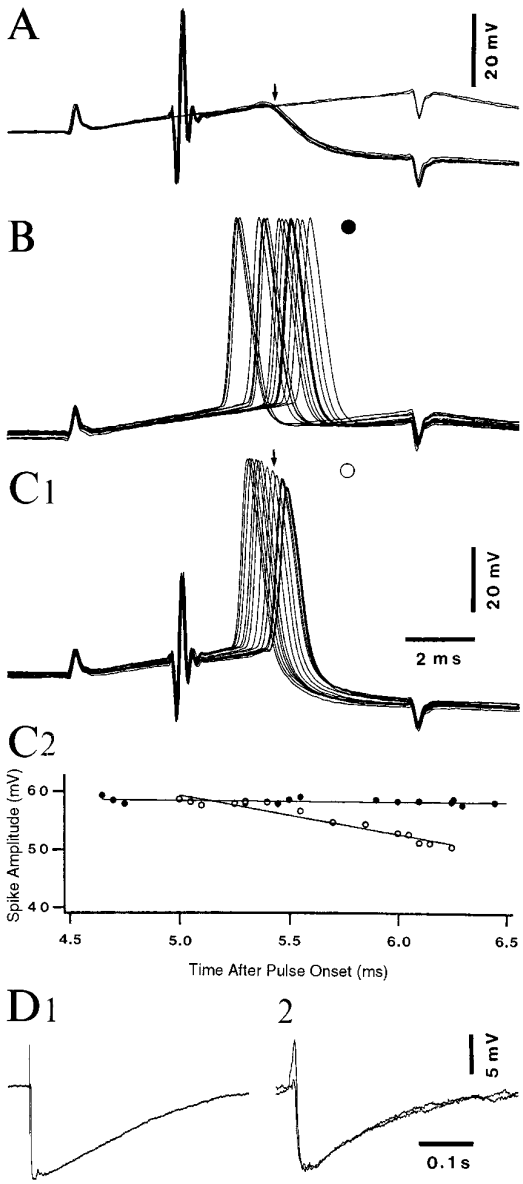

Fig. 7. Amplitude reduction of current-evoked spikes by cortically-evoked PSPs. Morphologically-identified layer III pyramidal neuron at rest (−66 mV). KAc-pipette. Panel A shows subthreshold responses to depolarizing current pulses (0.4 nA, 0.5 Hz) applied with or without cortical shocks. Panels B and C1 display suprathreshold responses to the same stimuli. In B, note constant amplitude of APs evoked by current injection alone. In C1, note progressive reduction in spike amplitude with increasing latency from cortical shocks. No orthodromic spikes were elicited after the time indicated by the arrow. The arrow in A points to the corresponding time in subthreshold trials. In C2, the amplitude of spikes elicited by current injection alone (filled circles) or in trials with cortical shocks (empty circles) is plotted as a function of time after pulse onset. With a slower time base, D1 depicts orthodromic responses to cortical shocks of the same intensity (average of 3). D2 depicts two EPSP–IPSP sequences that occurred spontaneously at the same V_m.

differences in the slopes of the depolarization triggering the APs, we also investigated the influence of sub-threshold cortical shocks on APs evoked by intracellular current pulses (n=10). The amplitude of these current pulses was adjusted to elicit spikes in 50% of the trials. As shown in Fig. 7B, the amplitude of the direct spikes remained constant in spite of

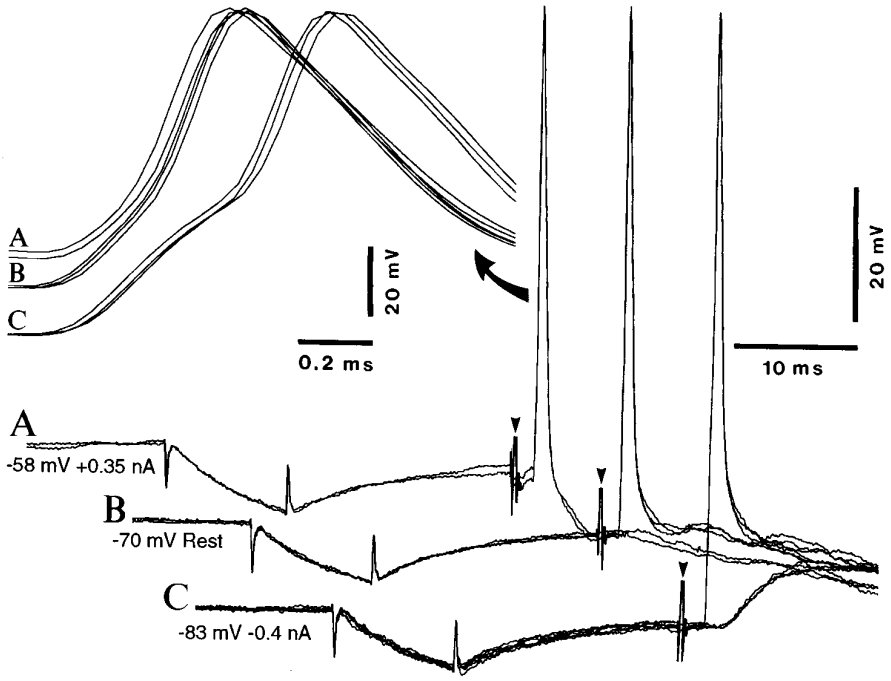

Fig. 8. Constant voltage peak of antidromic APs elicited from different V_ms. Morphologically-identified layer V pyramidal neuron backfired from a neighbouring cortical site. KAc pipette. Antidromic spikes were elicited at different V_ms as determined by intracellular current injection. Small current pulses were applied before the cortical shocks to insure that the bridge was balanced. Membrane hyperpolarization slowed the invasion of the somatodendritic compartment as manifested by the conspicuous break between the IS and somatodendritic spikes at -83 mV (C). Antidromic invasion began to fail at -83 mV and beyond, revealing cortically-evoked synaptic potentials at a longer latency. Note that the voltage peak of the antidromic spikes remained constant in the tested range of V_ms. The antidromic spikes are depicted with an expanded time base in the inset (curved arrow).

inter-trial variations in their latencies (Fig. 7B and C2, filled circles). In contrast, when cortical shocks were applied during the depolarizing current pulse, the spike amplitude progressively decreased (by up to 8 mV) as their latency increased (Fig. 7C1–2, empty circles). This phenomenon probably reflected the increasing impact of cortically-evoked PSPs on the recorded cell with time. In the example of Fig. 7, no spike was initiated after the time indicated by the arrow (Fig. 7C1). The corresponding time is indicated by an arrow on subthreshold trials depicted in Fig. 7A. Note that prior to this point, the cortically-evoked response had produced only small deviations from the voltage trajectory associated with the current pulse alone.

Relation between spike threshold and spike peak in ortho- and antidromic spikes

In CsAc (Fig. 3C, inset) and KAc (Fig. 6A) recordings of deep pyramidal neurons, orthodromic spikes elicited by deep cortical stimuli were consistently triggered at a lower V_m than spikes evoked by superficial cortical stimuli or by intracellular current injection. This difference was clearest when neurons were depolarized to just below threshold by intracellular current injection (Fig. 3). In such cases, the difference in spike threshold between orthodromic and current-evoked spikes averaged -5.2 ± 1.04 mV with deep stimuli and -2.1 ± 0.31 mV with shocks applied to mid-cortical layers (n=10). These differences were statistically significant (paired t-test, $P<0.05$). The threshold of APs evoked by superficial stimuli was not significantly different from that of direct spikes.

To verify if these subtle differences in spike thresholds influenced the spike amplitude, we investigated the effect of membrane polarization on the voltage peak of antidromic spikes in layer V pyramidal neurons recorded with KAc pipettes (n=6). As shown in Fig. 8, changing the V_m by up to 25 mV through intracellular current injection modified the spike peak by less than 1 mV. In Fig. 8C, note that the voltage peak of the antidromic spike remained constant even though the hyperpolarizing current induced a clear IS-SD break.

Effect of changes in the chloride gradient on the shape of orthodromic action potentials

Presumably, the depressing effects of orthodromic volleys on the APs generated by pyramidal neurons reflect local changes in R_{in} and V_m induced by the cortically-evoked PSPs. To assess the relative

importance of these two factors, pyramidal neurons were recorded with KCl (n=30) or CsCl (n=7) pipettes. Whereas in cells recorded with KAc or CsAc pipettes the IPSP reversals respectively averaged -78.1 ± 0.77 mV (n=4) and -73.8 ± 0.64 (n=4), in neurons recorded with KCl or CsCl pipettes they averaged -52 ± 2.89 mV (n=13) and -51 ± 2.13 mV (n=3), respectively. Chloride diffusion inside the cells thus caused a 20–25 mV shift in the IPSP reversal potential, bringing it close to the spike threshold.

The amplitude of current-evoked and orthodromic spikes generated by chloride-dialysed neurons was compared in two different paradigms. First, orthodromic spikes were elicited by cortical stimuli applied close to the soma level during short depolarizing current pulses previously adjusted to bring the V_m just below spike threshold. In this case, the intensity of the cortical shocks was adjusted to elicit spikes in 50% of the trials. In comparison to direct APs, the peak of the orthodromic spikes generated by neurons recorded with KCl-pipettes was reduced by 1.02 ± 0.23 mV (n=6), significantly less than the 6.3 ± 1.71 mV (n=5) reduction obtained in neurons recorded with KAc pipettes. However, because Cl^- diffusion reversed the IPSPs, a lower stimulation intensity, and presumably, a lower number of activated synapses, was required to elicit spikes thus leading to an underestimation of the impact of synaptic inputs on orthodromic APs in chloride-dialysed neurons.

To address this, orthodromic spikes were elicited from rest and the stimulation intensity was increased until no further decrements in spike amplitude could be produced. Using this approach, cortical shocks applied close to the somatic level reduced the spike peak by a maximum of 7.45 ± 1.22 mV (n=10) in neurons recorded with KCl pipettes. In comparison, threshold stimuli reduced the spike peak by 15.58 ± 1.24 (n=9) in cells recorded with KAc pipettes. Fig. 6 compares the spike reduction produced by deep cortical shocks in two pyramidal cells, one recorded with a pipette containing KAc (Fig. 6A) and the other with KCl (Fig. 6B). Note that even though threshold intensities were used in Fig. 6A, deep cortical shocks reduced the spike peak by 19 mV in the neuron recorded with KAc whereas the spike peak could not be reduced by more than 8 mV in the neuron recorded with KCl. Similarly, in neurons recorded with CsCl-pipettes (not shown), suprathreshold synaptic inputs could not reduce the spike peak by more than 6.5 mV compared to peak reductions of up to 18 mV produced by juxta-threshold cortical shocks in neurons recorded with CsAc-pipettes.

Computational models of neocortical pyramidal neurons

To investigate the mechanisms underlying the modification of the spike shape by synaptic inputs, a biophysical model of a layer V pyramidal neuron was constructed. As detailed in Experimental Procedures, this model was constrained by (i) morphological data about the differential distribution of symmetric and asymmetric synapses in the various cellular compartments,[8,62] (ii) biophysical findings concerning adult Na^+ channel densities in CA1 pyramidal neurons,[38] (iii) *in vivo* observations about R_{in} and repetitive firing, and (iv) *in vivo* findings about the differential features of synaptic responses evoked by cortical stimuli applied at different depths.

In order to provide a correct membrane time constant and R_{in}, the passive properties of the model cell were fitted to a recording of a deep pyramidal cell during injection of a hyperpolarizing current pulse. The fitting algorithm provided an optimal set of passive values, which was unique if no more than three parameters were simultaneously adjusted (see Experimental Procedures). Assuming uniform passive properties, the best fit gave values of g_{leak}= 0.7245 pS/μm^2, $E_{leak}=-68$ mV and R_i=200.1 Ohm cm when C_m was fixed at 1 μF/cm^2 (Fig. 9, Passive response). Slightly different values were obtained assuming lower values for C_m as in Ref. 41 or different dendritic corrections due to spines. Another fit was also performed assuming more compact dendrites and a larger leak in the soma to simulate damage due to the electrode impalement. No qualitative differences were found in the context of the present simulations (not shown).

Although voltage-dependent K^+ and Ca^{2+} currents, Ca^{2+}-dependent K^+ currents, and others shape the firing properties of pyramidal cells,[18,37,44,55] the frequency range of repetitive firing and adaptation could be approximated using I_{Na}, I_{Kd} and the non-inactivating K^+ current I_M (Fig. 9, repetitive firing, see Experimental Procedures). I_M was uniformly localized in the soma and dendrites, but similar firing patterns also occurred with I_M only located in the soma with a higher density. I_M was kept for all simulations shown in this study, even though its removal had no effects on the phenomena discussed here. In preliminary simulations, Ca^{2+} currents were inserted into the dendrites and soma with densities similar to those reported for hippocampal pyramidal cells.[38] Probably because these Ca^{2+} currents activate slowly in comparison to Na^+ currents, their presence did not affect the phenomena described below.

Simulation of synaptic inputs

As detailed in Experimental Procedures, two types of constraints were used in the simulations of the distribution of synaptic conductances activated by extracellular stimuli. First, the model incorporated the relative density of excitatory and inhibitory synapses available in different regions of pyramidal neurons as determined in previous ultrastructural studies.[2,8,14,15,29,49,62] Second, the fraction of synapses activated by a given stimulus was adjusted to

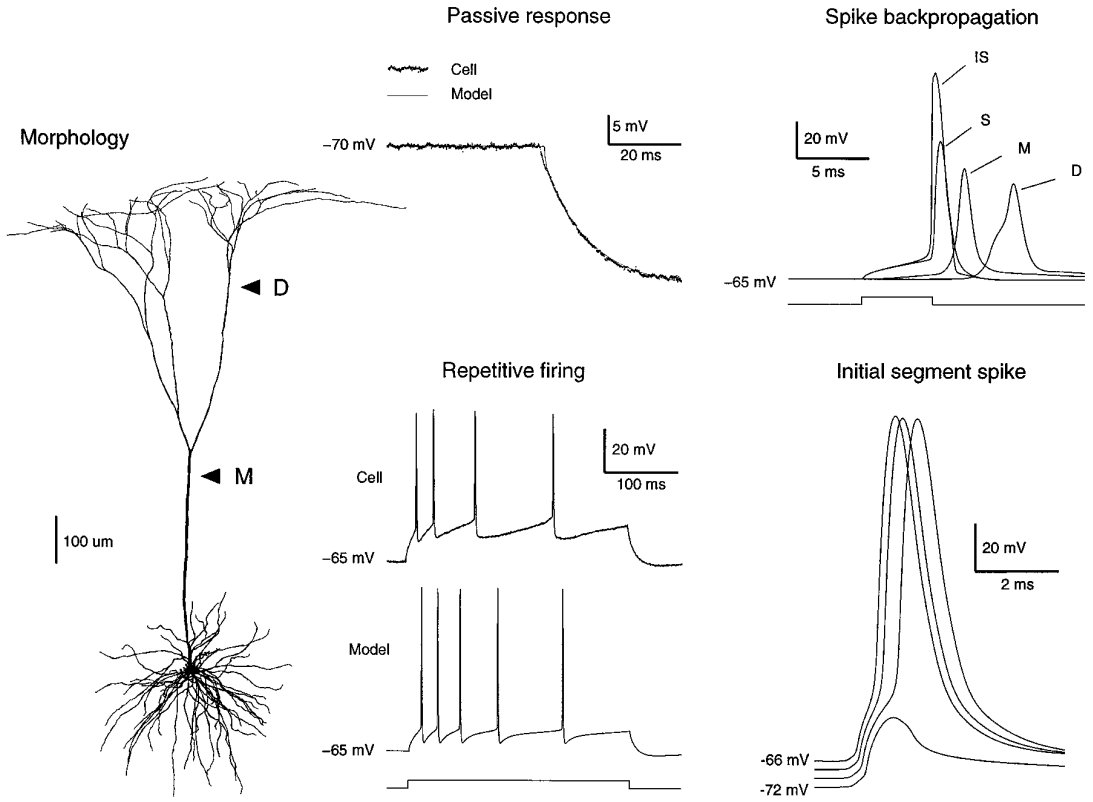

Fig. 9. Model of AP generation in layer V cortical pyramidal cells. Morphology: layer V pyramidal cell from cat neocortex digitized with a computerized tracing system and incorporated into the NEURON simulator. Passive response: To obtain the correct time constant and R_{in}, the passive properties of the model were fitted to *in vivo* intracellular recordings (average of 10 pulses of -0.38 nA applied at rest). Repetitive firing: active conductances (see Experimental Procedures) were inserted in the various cellular compartments. The top trace shows the response of a layer V cortical pyramidal cell *in vivo* in response to a current pulse of +0.5 nA (lower trace). A similar response was obtained in the model with leak, Na^+, Kd, and M currents (middle trace). Spike backpropagation: soma-to-dendrite propagation of an AP elicited by a depolarizing current pulse in the soma (IS, initial segment; S, soma; M, apical dendritic site ≈ 500 μm from soma; D, distal apical dendritic site ≈ 1 mm from soma). Initial segment spike: simulation of antidromic APs obtained by stimulating the axon. Somatic APs displayed minimal peak variation in the range of tested V_ms (obtained with d.c. current injection). For the most hyperpolarized level (-72 mV), the IS spike failed to invade the soma and appeared as a low-amplitude subthreshold event.

reproduce the differential electrophysiological features of synaptic responses observed experimentally in response to cortical stimuli applied at different depths. These features were, from deep to superficial cortical stimuli: (1) EPSP/IPSP amplitudes become progressively smaller; (2) EPSP/IPSP time courses become slower; (3) the delay between EPSP and IPSP onset increases; (4) the IPSP reversal potential shifts to more negative values; (5) the R_{in} drop decreases. We detail here how these electrophysiological features were used to constrain the density and distribution of activated synaptic currents in the model.

(1) The R_{in} change associated with the IPSPs elicited by proximal stimuli was dominated by the effect of inhibitory synapses ending on the soma and proximal 30 μm of the dendrites (compare traces in Fig. 10B, Proximal). Including EPSPs and IPSPs in more distal regions of the dendrites produced minimal changes in the response to proximal stimuli. This property allowed us to estimate the GABAergic conductance density necessary to account for these features: 60 pS/μm^2 in the soma and 17 pS/μm^2 in the dendrites. EPSP and IPSP amplitudes evoked by superficial stimuli could not be reproduced by assuming an entirely focal stimulus (Fig. 10B, Focal) as they were extremely attenuated, in agreement with previous studies.[1b,56,57] The only way to reproduce the *in vivo* observations was to assume an intermediate distribution of activated synapses where a cortical stimulus delivered at a particular depth activated a set of afferents preferentially ending at that depth, but also produced a less intense activation of afferent fibres ending at other levels (Fig. 10B, Overlap). The model reproduced responses to deep, intermediate and superficial cortical stimuli when the relative synaptic current densities of Proximal, Middle and Distal

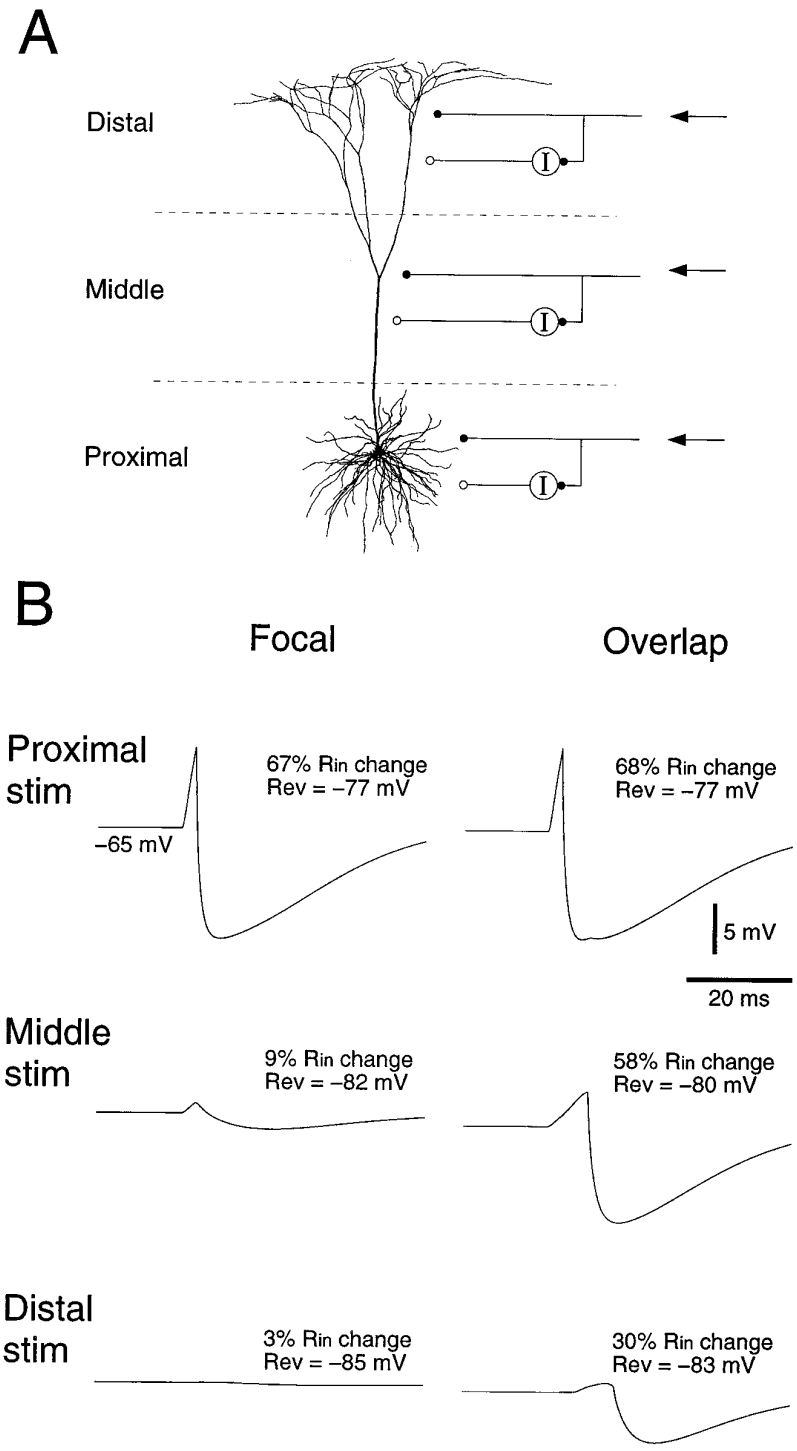

Fig. 10. Simulation of cortically-evoked EPSP/IPSP sequences assuming two different distributions of active synapses. (A) Scheme of synaptic stimulation in the model. The relative density of glutamatergic and GABAergic synapses in soma and dendrites was obtained from electron microscopic studies of neocortical pyramidal cells (see Experimental Procedures). The fraction of synapses activated by extracellular stimulation was estimated by dividing the cell into three regions (Proximal, Middle and Distal). Within each region, EPSPs and IPSPs were activated independently with a delay of 2 ms. (B) Somatic responses observed with two distributions of synaptic conductances. Focal: focal stimulation (synaptic currents activated in one region exclusively) could not reproduce the characteristics of EPSP/IPSP sequences observed *in vivo*. Overlap: EPSP/IPSP sequences observed when the electrical stimuli were assumed to activate synapses ending at a corresponding level, but also recruiting synapses contacting neighbouring regions with less intensity. In this case, electrophysiological features such as IPSP amplitudes, time-to-peak, R_{in} changes and reversal potential, could be reproduced (see details in text). Synaptic conductance densities were: 60 pS/μm^2 for $GABA_A$ in soma, 17 pS/μm^2 for $GABA_A$ in dendrites and 13 pS/μm^2 for AMPA and NMDA in dendrites. The latter corresponds to EPSPs just below threshold for APs.

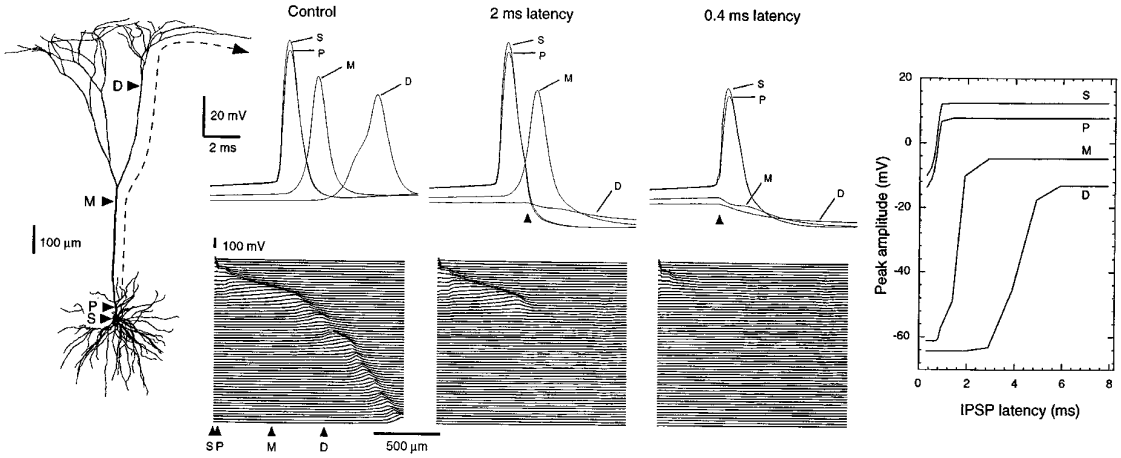

Fig. 11. IPSPs reduce the somatic AP amplitude. Injection of a short current pulse (+0.5 nA) in the soma evoked a spike, which is shown in the absence of an IPSP (Control), with an IPSP starting during its decaying phase (2 ms latency) or during its rising phase (0.4 ms latency). A "proximal" IPSP was used for these simulations (see Experimental Procedures for details). For each condition, the V_m is shown at the somatic (S), proximal dendritic (P), mid-apical dendritic (M) and distal apical dendritic levels (D; arrowheads in the cell drawing show location of measurements). The bottom panels depict the V_m profile along a pathway starting from the soma and ending in the most distal dendrites (path indicated by a dotted line in the cell drawing). The plot was made over a period of 12 ms in steps of 0.2 ms starting from AP initiation (from top to bottom). The rightmost panel plots the spike amplitude at the different dendritic and somatic sites as a function of the IPSP latency.

compartments were adjusted to 1:0.5:0.25, 0.5:1:0.5 and 0.25:0.5:1, respectively.

(2) The IPSP reversal potential, time to peak and R_{in} drop produced by middle and distal stimuli depended highly on the GABAergic and glutamatergic conductance densities. Assuming that the fraction of GABAergic synapses activated by middle and distal stimuli was equal to that evoked by proximal stimuli, we estimated a glutamatergic conductance density of $\approx$13 pS/µm^2.

(3) To reproduce the timing of EPSP–IPSP sequences, we had to assume that most glutamatergic and GABAergic synapses were not activated simultaneously. In our experiments, responses to proximal stimuli were characterized by a delay of $\approx$2 ms between EPSP and IPSP onsets (Fig. 5A). This suggests that extracellular stimuli recruited excitatory fibres that directly contacted the recorded cell as well as inhibitory interneurons, thus leading to an IPSP delayed by about 2 ms. In our model, this phenomenon was simulated by introducing a delay of 2 ms between the activation of glutamatergic and GABAergic conductances (Fig. 10B, Proximal stim). The same delay (2 ms) was also necessary to model EPSP–IPSP sequences generated in cortical pyramidal cells by thalamic inputs.[6a]

(4) Simulating Distal stimuli required a more complex pattern of activation. In this case, the experimentally observed delay between EPSP and IPSP onsets was $\approx$10 ms. In keeping with the above (4), we assumed that within each compartment the IPSP onset was delayed by 2 ms with respect to the EPSP. However, the activation of successively more proximal compartments was delayed further (in Fig. 10B, Distal stim was obtained with distal EPSP at 0 ms; distal IPSP at 2 ms; middle EPSP at 4 ms; middle IPSP at 6 ms; proximal EPSP at 8 ms; proximal IPSP at 10 ms). This pattern of activation would correspond to complex polysynaptic pathways recruiting synapses at different levels of the neuron.

(5) To sum up, the differential electrophysiological features of synaptic responses evoked by extracellular stimuli applied at different depths could be reproduced by families of distributions that assumed the same temporal relationship, the same relative conductance densities and the same degree of overlap between different levels. Fig. 10B (right panels) illustrates simulations using the optimal values that we found for these parameters. They are in excellent agreement with the data shown in Fig. 5.

Effect of inhibitory postsynaptic potentials on simulated action potentials

To study the effects of IPSPs on APs, a depolarizing current pulse was injected at the soma level and "proximal" IPSPs (see Experimental Procedures) were applied at various delays after the spike onset (Fig. 11). Obviously, such pure proximal IPSPs rarely occur in reality, but this extreme case was used to simplify the analysis of the mechanisms underlying spike reductions by IPSPs. The IPSP amplitude and

reversal potential (−78 mV) were adjusted to match those of spontaneously occurring IPSPs (Fig. 7D2). The amplitude and propagation of APs were visualized with dendritic profiles (bottom graphs in Fig. 11) depicting the V_m from the soma (S) to the distal (D) apical dendrites (horizontal axis) in 0.2 ms steps (vertical axis).

When no IPSPs were applied (Fig. 9, Spike backpropagation), APs evoked by current injection were initiated in the IS, and then propagated actively to the soma and dendritic tree. The peak of the antidromic spikes was largely independent of the holding level (Fig. 9, Initial segment spike) until sufficient hyperpolarization prevented the activation of the soma by the IS spike. The spike did not propagate at a constant velocity in the dendrites, but decelerated as the diameter of the successive dendritic segments decreased (Fig. 11, Control). For instance, the spike propagated at ≈0.4 m/s in the apical trunk, at ≈0.2 m/s following the first branching point, and at ≈0.1 m/s in the apical tuft. As a result, a delay of approximately 10 ms elapsed between the somatic APs and its retrograde propagation in the distal apical tuft. In addition, the amplitude of propagating spikes decreased at dendritic branching points, in agreement with previous theoretical findings,[16a] making the active invasion of dendrites especially sensitive to inhibitory synaptic inputs affecting these dendritic regions (see below).

Proximal IPSPs did not alter the shape of the somatic APs unless they coincided with the propagation of the spike in the proximal dendritic segments (0–150 μm). For instance, in trials where the IPSPs occurred after the AP had propagated in the apical trunk up to the first branching point (Fig. 11, 2 ms latency), the somatic spike was unchanged in spite of the propagation failure in more distal dendritic segments (D). However, with shorter delays (Fig. 11, 0.4 ms) where the IPSP onset occurred before or during the spike propagation in the proximal dendritic segments (P), the somatic spike was reduced in amplitude by up to 25 mV and the spike failed to invade the dendrites. The graph on the right of Fig. 11 illustrates the relation between the spike peak in different cellular compartments and the timing of the IPSP. It should be pointed out that reductions in somatic AP amplitudes were not always accompanied by a failure of backpropagation. However, large IPSPs that produced important (>20 mV) somatic spike reductions always prevented backpropagation in our simulations.

The minimal proximal IPSP amplitude required to block the activation of dendritic spikes was dependent on the dendritic Na^+ channel density and was in the range of 5–10 mV in the example above. The Na^+ conductance density used here (70 pS/μm^2) corresponds to the highest somatic/dendritic densities found in pyramidal cells.[38] Decreasing the Na^+ channel density dramatically increased the sensitivity of dendritic spikes to IPSPs (not shown).

Mechanisms of somatic spike reductions by inhibitory postsynaptic potentials

To determine how local changes in R_{in} and V_m contributed to reduce the amplitude of the somatic spike, we studied the effects of changing the IPSP reversal potential while keeping the GABAergic conductance constant. Figure 12A shows a plot of the spike peak as a function of the IPSP reversal potential. Shifting the reversal potential from −12 mV to −56 mV progressively reduced the peak of the somatic spike without preventing the active invasion of the AP in the dendrites (Fig. 12A2, black dots). For instance, when the IPSP reversal was set to −55 mV, close to the spike threshold, the spike peak was reduced by 12 mV (Fig. 12A1). However, note that the spike duration was not decreased (Fig. 12A1). Further negative shifts in reversal potential eventually prevented the active invasion of the spike in the dendritic tree (crosses) as reflected by the increased slope of the curve between −60 and −80 mV (Fig. 12A2). These results suggest that the conductance increase due to the opening of $GABA_A$ receptors only accounts for part of the total spike amplitude reduction. Therefore, additional voltage-dependent mechanisms must be considered.

To determine the contribution of dendritic Na^+ currents to the somatic spike, Na^+ channels were removed from the most distal dendritic segments to progressively more proximal dendritic levels. Fig. 12B2 plots the peak of the somatic spike as a function of the distance from the soma up to where Na^+ channels were present. In control conditions, the spike peak was reduced only when Na^+ channels were removed from the proximal segments of the dendrites (<200 μm). When all Na^+ channels were removed from the dendrites, the spike amplitude was reduced by 9.3 mV. This indicates that the sensitivity of the spike peak to the removal of dendritic Na^+ channels is not only determined by the electrotonic length of the cell but also by what segment of the dendrites is invaded by the propagating AP when the peak of the somatic spike occurs. However, the importance of the electrotonic length in determining the sensitivity of the somatic spike to the removal of Na^+ channels was demonstrated by eliciting, immediately after the onset of the AP, an IPSP whose reversal was set at −55 mV. In this condition, the peak of the somatic spike was sensitive to the removal of Na^+ channels over a smaller dendritic segment (proximal 150 μm; Fig. 12B). Therefore, these observations suggest that the Na^+ currents in the proximal dendrites significantly contribute to the somatic spike. This effect, combined with the conductance increase related to IPSPs, accounts for most of the spike amplitude reduction (Fig. 12B1, No dendritic Na+IPSP rev −55 mV).

The contribution of dendritic Na^+ channels to somatic spikes was further assessed by comparing the amplitude of somatic and dendritic Na^+ currents

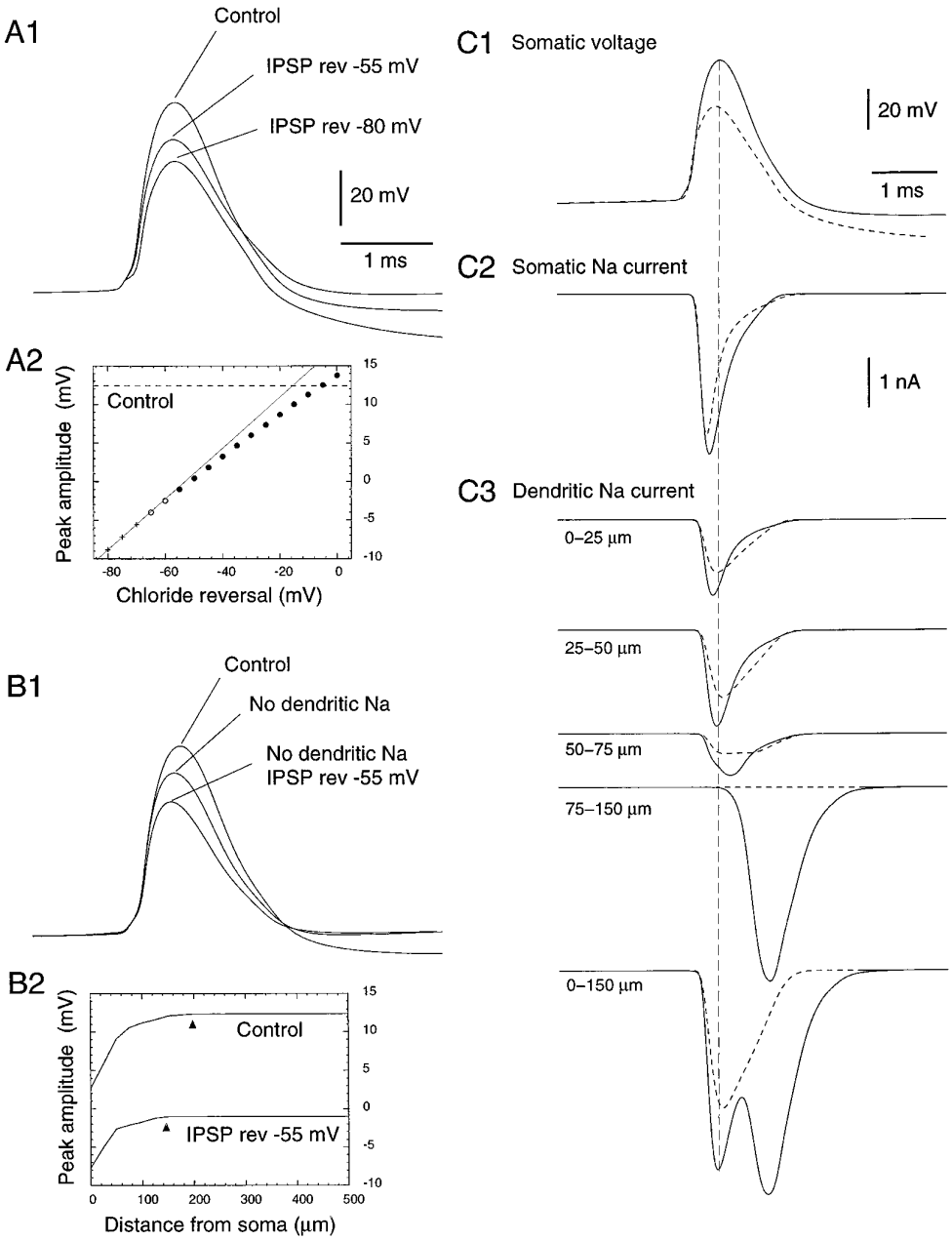

Fig. 12. Mechanisms of spike amplitude reduction by IPSPs. (A) Amplitude reduction due to conductance shunt. (A1) Superimposed APs elicited by intracellular current injection shown in the control condition (Control) and in the presence of proximal IPSPs with different reversal potentials (−55 mV, −80 mV). (A2) Plot of the somatic spike peak as a function of IPSP reversal potential. Symbols indicate IPSP reversals that allowed (filled circles), prevented (crosses) or limited (empty circles) the active invasion of the dendrites by the somatic spike. (B) Amplitude reduction due to removal of dendritic Na^+ currents. (B1) Removal of all dendritic Na^+ channels reduced the spike amplitude (Control) to an intermediate level (No dendritic Na^+). If this effect is combined with the conductance shunt of the IPSP (No dendritic Na^+, IPSP rev −55 mV), the total reduction obtained is similar to the spike reductions observed experimentally. (B2) Plot of somatic spike peak as a function of distance from the soma where Na^+ channels were present. Na^+ channels were present from the soma up to the indicated distance. (C) Participation of dendritic Na^+ currents in somatic APs. (C1) Somatic spikes elicited by current injection in the control condition (continuous lines) and in the presence of an IPSP (dashed lines). (C2) Total somatic Na^+ current in the same conditions. (C3) Total Na^+ current of dendritic regions at progressively increasing distances from the soma. Total current was calculated by summing the instantaneous Na^+ current in each compartment within the indicated distance range. The amplitude of the "control" somatic spike in the soma correlates with significant Na^+ current in proximal dendrites. When spike amplitude is reduced, the dendritic Na^+ current is dramatically reduced.

during control spikes versus IPSP-reduced APs (Fig. 12C). In control conditions (Fig. 12C, continuous lines), a significant dendritic Na^+ current (up to about 75 μm from soma) coincided with the somatic spike. In the presence of an IPSP (Fig. 12C, dashed lines), dendritic Na^+ currents were significantly reduced. Note that the discrepancy between the length of the dendritic segment contributing to somatic AP in Fig. 12B and C is probably due to alterations in the electrotonic structure of the model caused by removing dendritic Na^+ channels in Fig. 12B.

Effects of inhibitory postsynaptic potentials on the dendritic invasion of spikes

To determine how sensitive the dendritic contribution to somatic spikes is, inhibitory synapses distributed throughout the cell surface were activated immediately after the onset of a current-evoked AP. Weak activation of inhibitory synapses producing a somatic hyperpolarization <2 mV did not prevent the invasion of the dendrites by the somatic AP, but reduced its propagation velocity (Fig. 13B–C). However, IPSPs producing a somatic hyperpolarization ≥2 mV prevented the spike propagation beyond the first branching point (Fig. 13D–F), and large IPSPs (around 10 mV and more) prevented the activation of Na^+ spikes in the proximal dendritic segments and beyond (Fig. 13G–H). The above results show that even weak IPSPs, distributed throughout the cell surface, are able to affect significantly the invasion of dendrites by APs. However, an early suggestion was that strategically placed IPSPs could selectively prevent the invasion of specific dendritic branches.[32a] In the present model, focally-applied IPSPs could perform such a selective shut-off of dendritic branches (not shown) with little or no somatic hyperpolarization, and no detectable effect on somatic spike amplitude. This observation parallels the results of focally-applied distal IPSPs on hippocampal pyramidal cells *in vitro*, where no prominent effects on somatic spike amplitude were seen.[61]

Synaptically-evoked spikes

To determine whether the mechanisms of spike amplitude reduction by pure IPSPs also apply to spikes elicited by synaptic stimulation, the excitatory conductance obtained for subthreshold EPSP/IPSP sequences (Fig. 10) was gradually increased until the synaptic stimulation became just suprathreshold. Stimuli at Proximal, Middle or Distal levels became suprathreshold when the density of glutamatergic conductances was increased from 13 to 18 pS/μm^2 with unchanged inhibitory conductances.

In these conditions, the model reproduced the progressive spike amplitude reductions that were observed experimentally as a function of stimulation depth. Figure 14A illustrates this phenomenon for various "recording" conditions. In control conditions (Fig. 14A, KAc), spikes elicited by somatic current injection (Direct) were of the highest amplitude and duration, followed by Distal to Proximal stimulation, in agreement with our experimental observations (compare Fig. 14A, KAc, with Fig. 6A). The smaller AP reductions observed experimentally with KCl pipettes could also be reproduced in our simulations by setting the chloride equilibrium potential at −55 mV (compare Fig. 14A, KCl, with Fig. 6B). To simulate recordings with CsAc pipettes, we included high-threshold Ca^{2+} currents and Ca^{2+}-dependent K^+ currents in the soma and dendrites (see Experimental Procedures and Appendix). Supra-threshold stimuli applied in these conditions reproduced the differential reductions in spike amplitude and duration that were observed experimentally as a function of stimulation depth (compare Fig. 14A, CsAc, with Fig. 3C).

Manipulating the IPSP reversal potential and dendritic Na^+ channels as shown in Fig. 12 revealed that the mechanisms underlying the spike reduction by EPSP–IPSPs sequences are similar to those documented for pure IPSPs. However, in the CsAc condition, dendritic Na^+ channels up to 300 μm from the soma were found to provide an important contribution to the falling phase of APs (not shown).

Dendritic profiles in Fig. 14B show that in simulations reproducing KAc conditions, cortical stimuli applied at perisomatic levels elicited APs that were initiated in the IS, propagated to the soma, but failed to invade the dendritic tree. In comparison to current-evoked spikes, the amplitude of these APs was reduced by 17 mV, very close to the experimentally observed average reduction. In our model, distal cortical shocks could only elicit somatic spikes when the afferent volley first triggered a dendritic spike (Fig. 14C). This is in agreement with previous intracellular studies of neocortical pyramidal cells *in vivo* and *in vitro*[5,9,30,52] where it was observed that synaptic stimuli can elicit dendritic spikes (reviewed in Ref. 66). However, it should be noted that our model was designed to reproduce *in vivo* observations obtained with electrical stimuli applied to the cortex and included the activation of GABAergic synapses at the soma level, a phenomenon that may not occur in natural conditions. In our model, these synaptically-evoked dendritic spikes propagated to the soma, but the resulting somatic spike did not retrogradely invade the dendrites because of Na^+ channel inactivation. Compared to current-evoked spikes, the amplitude of APs elicited by distal inputs were reduced by only 1.4 mV.

Effects of changes in the parameters of the model

The simulations illustrated so far used a single set of parameters that could reproduce the intracellular data collected in our *in vivo* experiments. However, as the conclusions of the model might be sensitive to the

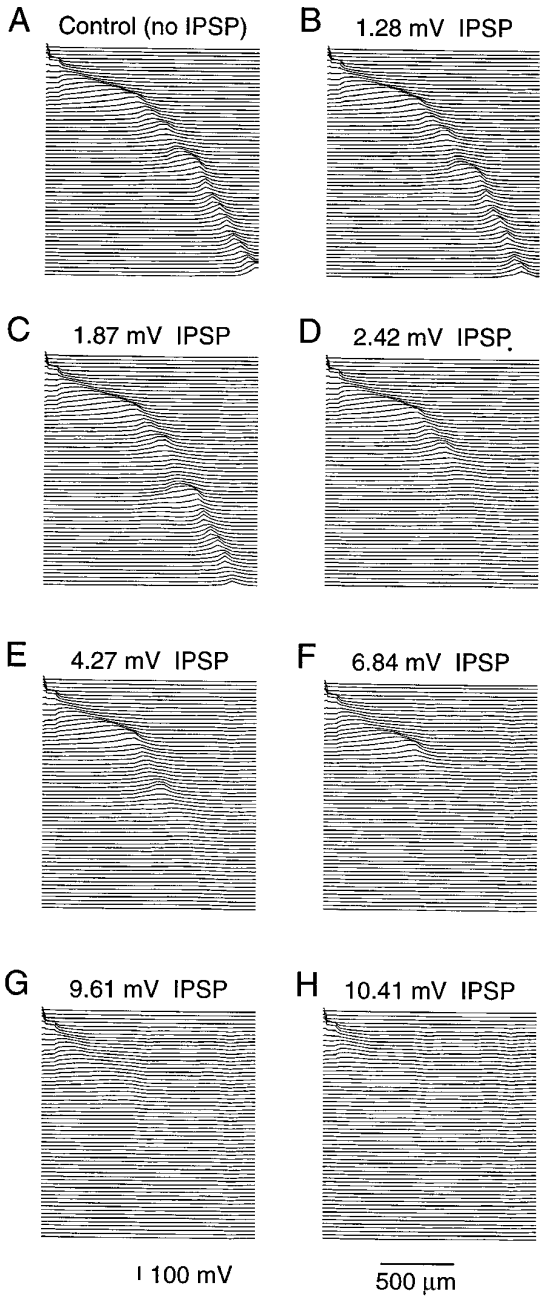

Fig. 13. Effect of IPSPs of different strengths on the somatodendritic V_m profile during direct APs. In control (A), no IPSP was present. In panels B–H, IPSPs of increasing amplitude were applied immediately after spike initiation. IPSPs were simulated with a uniform GABAergic conductance density in dendrites. The number on the top of each panel indicates the peak amplitude of the IPSP at the soma. Weak IPSPs slowed the dendritic spike invasion (conductances of 0.5 and 0.75 pS/µm^2 for B and C, respectively). D–F: IPSPs larger than 2 mV at the soma progressively limited spike invasion in distal dendrites (conductances of 1, 2 and 4 pS/µm^2 for D, E, and F, respectively). G–H: larger IPSPs prevented the propagation of the somatic spike in the proximal dendrites (GABAergic conductances were of 8 and 10 pS/µm^2 for G and H, respectively). Somatodendritic V_m profiles were calculated as in Fig. 11. These IPSPs decreased the R_{in} by 6.9% in B, 9.5% in C, 12.4% in D, 22.1% in E, 35.9% in F, 51.5% in G and 57.1 in H.

specific parameters that were selected, additional simulations were performed to address the following issues.

Is the phenomenon of spike reduction sensitive to the distribution of synaptic currents? So far, we have explored distributions of EPSPs and IPSPs constrained by previous ultrastructural findings and our own electrophysiological data. Although these EPSP/IPSP distributions provide a plausible explanation for spike reduction, other distributions also led to the same conclusion. For example, proximal inhibition alone reduced the somatic spike amplitude and limited its invasion in dendrites. However, if perisomatic inhibition was strictly concentrated to the soma, the spike amplitude was only partially reduced. Full spike amplitude reduction required that IPSPs also affect the first 100 µm of proximal dendrites.

Is somatic spike reduction by IPSPs sensitive to the distribution of Na^+ channels? Simulations using different Na^+ channel distributions, such as a uniform density in all compartments including the axon, also showed spike amplitude reductions caused by IPSPs. In these simulations, the peak amplitude of current-evoked somatic spikes also coincided with the rise of the AP in the proximal dendrites so that dendritic Na^+ currents contributed to the somatic spike amplitude (Fig. 12C). With higher densities of dendritic Na^+ channels, stronger IPSPs were needed to reduce the spike amplitude, but in all cases, somatic spike reductions were accompanied by a reduced participation of proximal dendritic Na^+ currents. The dendritic Na^+ channel density chosen for the illustrations was conservative, in the upper range for adult CA1 pyramidal neurons,[38] thus making the participation of dendritic Na^+ channels to somatic spikes more resistant to IPSPs. Somatic spikes were significantly more sensitive to IPSPs when lower densities of dendritic Na^+ channels (about 30 pS/µm^2) were used.

What is the role of the IS in this model? The model had an increased Na^+ channel density in the axon IS, similar to previous models[1a,41] but much higher than that experimentally determined for the IS of subicular neurons.[5a] This feature was required for the following reasons. (1) Pyramidal cells having a low Na^+ channel density in soma and dendrites,[38] in the range of 20–70 pS/µm^2, do not generate overshooting somatic APs unless there is a region of increased Na^+ channel density (around 20,000–50,000 pS/µm^2) that is electrotonically close to the soma. (2) The features of AP reduction by synaptic stimulation observed experimentally could be accounted for by our model with an increased Na^+ channel density in either the IS or the axon (not shown), in agreement with a previous model.[51] Taken together, our experimental and modelling observations are consistent with a model of the pyramidal neuron in which there is a low density of Na^+ channels in the soma and dendrites and a high density in a region electrotonically close to the soma, such as the axon or IS. Whether APs initiated in the IS or in the axon had no influence on

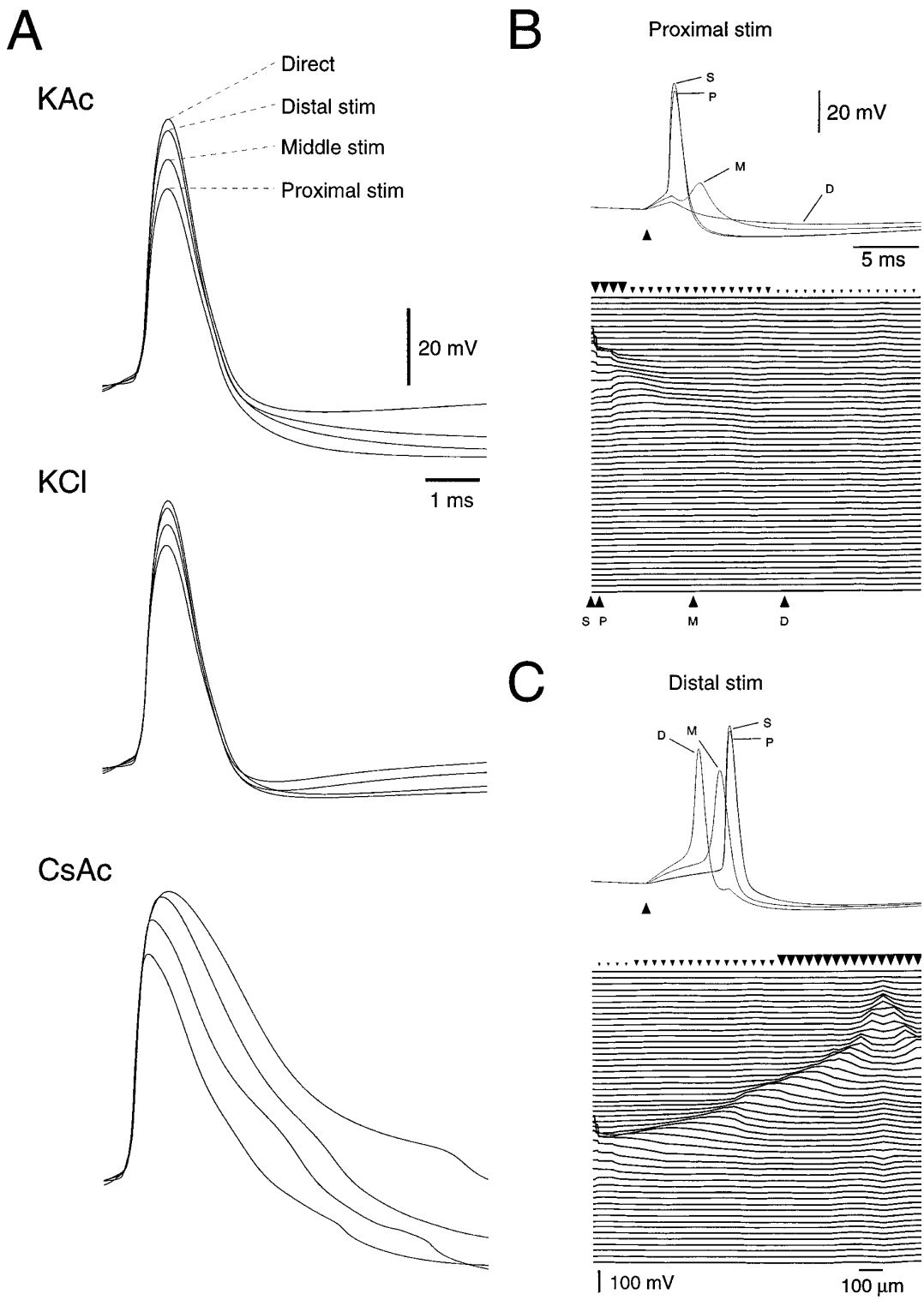

Fig. 14. Reduction of somatic spike amplitudes by synaptic stimulation. (A) Somatic spike elicited by current injection (Direct) and compared to APs evoked by synaptic stimulation at different "depths" (Distal, Middle, Proximal). Three recording conditions are simulated: control (KAc; see Fig. 6A), with an IPSP reversal of −55 mV (KCl; see Fig. 6B) and under Cs (CsAc; see Fig. 3). Proximal stimulation elicited spikes of reduced amplitude and width. In the latter simulation, K^+ currents (I_{Kd}, I_M) were blocked at 95% and high threshold Ca^{2+} currents (I_{CaH}) were included (see details in text). In this case, the broader spikes also showed progressive amplitude and width reductions with increasing stimulation "depths". (B) Dendritic membrane potential profile during proximal stimulation (same simulation as in A, KAc, Proximal stim). The spike initiated close to soma, but did not invade more distal dendrites. (C) Dendritic membrane potential profile during distal stimulation (same simulation as in A, KAc, Distal stim). In this case, distal stimulation produced a dendritic Na^+ spike that propagated towards the soma and elicited a somatic AP. Dendritic profiles in B–C were constructed as in Fig. 11; arrowheads above show the location and relative intensity of the synaptic inputs (see text).

the mechanisms of spike reduction reported here, as they involve somatodendritic interactions.

DISCUSSION

By combining *in vivo* intracellular recordings and computational models of neocortical pyramidal neurons, we obtained evidence suggesting that (i) Na^+ currents in proximal dendrites have an important influence on the shape of somatic APs; (ii) IPSPs of sufficient amplitude can prevent the participation of dendritic Na^+ currents, leading to somatic spikes of reduced amplitude and duration. In the following account, we will consider the mechanisms underlying the influence of IPSPs on spike genesis and discuss their implications for somatofugal spike propagation.

Cortical microstimuli applied at different depths preferentially activate synaptic inputs ending on different cellular compartments

Extracellular microstimuli applied at different cortical depths were used to activate synaptic inputs to pyramidal neurons. Several observations suggest that these stimuli activated synaptic inputs preferentially ending on particular segments of the somatodendritic axis and that this phenomenon was responsible for the differential modification of the spike shape by cortical stimuli applied at different depths. First, a systematic relation was found between the soma depth and the stimulation sites most effective in modifying the spike shape: for deep and superficial pyramidal neurons, cortical stimuli applied at the soma level were most effective. This is probably related to the fact that the soma, proximal dendrites and initial axonal segment of pyramidal neurons only receive inhibitory synapses[8,62] and that electrical stimuli applied at the soma level are more likely to activate these inhibitory fibres.

Second, IPSPs elicited by deep stimuli in layer V pyramidal neurons had larger amplitudes, were associated with higher R_{in} drops, but had less polarized reversal potentials than IPSPs evoked by superficial cortical stimuli. These features suggest that fibres recruited by deep stimuli end at sites that are electrotonically closer to the soma than synapses mediating the effects of superficial stimuli.

Third, in our computer simulations, assuming that cortical stimuli recruited inputs targeting a focal region of the dendritic tree or assuming a non-specific distribution of activated inputs failed to account for the observed features of EPSP/IPSP sequences. The only way to reproduce the differential features of cortically-evoked IPSPs as a function of stimulation depth was to assume that a cortical stimulus delivered at a particular depth activates a set of afferents that preferentially ends at a corresponding depth, but also produces a less intense activation of fibres ending at other levels.

Mechanisms underlying spike reductions by inhibitory postsynaptic potentials

Considered together, our experimental data and biophysical simulations suggest that two main factors explain the somatic spike reductions by IPSPs. First, there is a shunt effect due to the opening of $GABA_A$-receptor channels. Second, IPSPs reduce the contribution of proximal dendritic Na^+ currents to the somatic spike. Evidence for the shunting effect of IPSPs was obtained in neurons recorded with KCl pipettes where it was observed that IPSP still reduced the spike amplitude even though the IPSP reversal was around -50 mV. In these conditions, however, the effect of IPSPs on spike amplitude, although still present, was markedly attenuated, suggesting that another factor, this one voltage-dependent, was involved. Evidence for this second mechanism was obtained in computer simulations where it was found that (i) in control conditions, somatic spikes contain a significant contribution of proximal dendritic Na^+ currents, up to about 100 μm from the soma; (ii) IPSPs prevent or diminish this contribution, leading to a reduced somatic spike amplitude. These considerations suggest that proximal IPSPs of increasing strength lead to a progressive reduction in spike amplitude by "knocking out" larger portions of dendrites. Thus, the progressive recruitment of proximal IPSPs from distal to proximal stimuli probably explains the increasing spike reductions observed from distal to proximal stimulations. However, it should be pointed out that in our experiments, IPSPs were elicited by electrical shocks. This type of stimulus may produce an artificially synchronous activation of inhibitory fibres. Yet, spontaneous IPSPs with amplitudes comparable to those of evoked IPSPs were observed, which also altered somatic spikes (Figs 3A2, 7D2).

Influence of inhibitory postsynaptic potentials on somatofugal spike propagation

Our models suggest that during a spike elicited by current injection, the peak of the somatic AP coincides with the rising phase of I_{Na} in the proximal dendrites. Hyperpolarizing IPSPs of sufficient amplitude can counteract the rise of I_{Na} in the proximal dendrites and thereby reduce the somatic spike amplitude. Thus, the present experiments and models suggest that the somatic spike shape provides a "window" into the participation of the proximal 100 μm of the dendrites.

A better insight into active dendritic events was obtained in neurons recorded with CsAc pipettes. By blocking I_{Kd} and some Ca^{2+}-dependent K^+ currents,[20,65] Cs^+ reduced the R_{in} drop normally occurring during the spike repolarization thus maximizing the dendritic depolarization caused by the somatic spike and allowing the soma to "see" more of the active dendritic events triggered by the AP. As a result, APs generated by Cs^+-filled pyramidal

neurons were prolonged by a shoulder that lengthened their falling phase. In inferior olivary cells, this shoulder is mediated by high-threshold dendritic Ca^{2+} currents.[35,36] Since pyramidal cells possess similar dendritic conductances,[30,67] and pyramidal neurons generate dendritic Ca^{2+} plateaus in the presence of K^+ channel blockers,[53,67] a similar mechanism probably contributed to the spike shoulder observed here.

In computer simulations of Cs^+ recordings, it was determined that Na^+ currents generated by the proximal 300 μm of the dendrites contributed to the falling phase of the somatic APs. Proximal IPSPs could reduce or prevent this contribution provided that they were correctly timed with respect to the activation of proximal dendritic Na^+ channels. In light of these considerations, the dramatic reduction of the Cs-induced spike shoulder and prolonged plateaux by cortically-evoked IPSPs suggests that the activation of dendritic Na^+ and Ca^{2+} conductances by backpropagating APs can be controlled by synaptic events.

Much experimental and computational data supports this conclusion. For instance, Kim *et al.*[31] showed that IPSPs can reduce or block current-evoked Na^+ and Ca^{2+} dendritic spikes in neocortical pyramidal neurons maintained *in vitro*. That back-propagating APs are sensitive to IPSPs was also observed in a recent experimental study of CA1 pyramidal neurons *in vitro*.[61] In this study, IPSPs produced no reductions in somatic spike amplitude because they were elicited by stimulation of stratum lacunosum-moleculare and targeted the distal dendrites. This is consistent with our simulations where the invasion of specific dendritic branches by back-propagating APs could be prevented by locally activating inhibitory synapses in distal dendrites, with no effect on the somatic spike.

Two modelling studies addressed the influence of synaptic events on spike back-propagation and provided support for the idea that this phenomenon can be modulated by synaptic inputs. In a conference abstract describing a modelling study of neocortical pyramidal neurons,[1a] it was observed that dendritic spiking and spike back-propagation can be controlled by IPSPs even though the density of dendritic and somatic Na^+ channels was three-fold higher than in our model. In the other study, it was found that backpropagating APs can be modulated in a graded manner by background synaptic activity, but that only powerful inputs can dampen them in a significant way.[51]

The sensitivity of backpropagating APs to synaptic control should not come as a surprise. In spite of developmental increases in the number of Na^+ channels, the density of Na^+ channels in the dendrites remains relatively low[24,38] and dendritic Na^+ spikes are weakly regenerative.[27] As a result, the dendritic propagation of somatic APs is vulnerable to a variety of factors. For instance, recent *in vitro* experiments on CA1 pyramidal neurons showed that only the first few APs of a spike train fully invade the dendritic tree,[4,58] a phenomenon that was ascribed to Na^+ channel inactivation or to the activation of K^+ channels.[45a,58] Similarly, in unanaesthetized rats, dendritic invasion of successive APs is significantly reduced during spike bursts generated by CA1 pyramidal neurons during slow wave sleep[3a]. Moreover, in neocortical pyramidal neurons observed *in vivo* with two-photon excitation laser scanning microscopy,[59a] spike-related increases in Ca^{2+} concentration were reported to be limited to the proximal apical dendrites.

Limitations of the model

Although the conclusions of our simulations showed a remarkable robustness to variations in the model's parameters, several points remain to be addressed. First, the passive properties of pyramidal neurons may not be uniform because of the presence of background synaptic bombardment *in vivo*. To limit this effect, we have performed recordings under deep barbiturate anaesthesia where spontaneous network activities are reduced. Comparing experimental data and simulations of the same cellular geometry should also greatly help in constraining these passive parameters. Second, various components of the model were based on data from other types of neurons as it was not available for adult neocortical pyramidal cells. Here, the availability of appropriate experimental data should help to further constrain the model. The data needed are: (i) the localization and density of Na^+ channels in different regions of the cell of adult neocortical pyramidal cells, including the soma, axon and initial segment; (ii) the exact details of Na^+ channel kinetics in adult neocortical pyramidal cells at body temperature; (iii) the distribution and kinetics of K^+ channels in dendrites. We found here that distributing IKd uniformly, like Na^+ channels, gave the most consistent results. This observation also awaits experimental verification.

Conclusions

Our experimental evidence and biophysical simulations suggest that Na^+ currents generated by the proximal dendrites contribute significantly to somatic spikes and that perisomatic IPSPs can reduce or prevent this dendritic contribution through a shunt and a voltage-dependent effect. It is suggested that IPSPs can modulate the retrograde propagation of somatic spikes in the dendrites provided that they are of sufficient amplitude and timed correctly.

Acknowledgements—This work was supported by grants from NSERC, MRC and FRSQ. E. J. L. supported by a NINDS post-doctoral fellowship.

REFERENCES

1. Angelides K. J., Elmer L. W., Loftus D. and Elson E. (1988) Distribution and lateral mobility of voltage-dependent sodium channel in neurons. *J. Cell Biol.* **106,** 1911–1924.
1a. Beierlein M. and Connors B. W. (1995) Differential control of excitable dendrites by inhibition in neocortical pyramidal cells. *Soc. Neurosci. Abstr.* **21,** 2445.
1b. Bekkers J. M. and, Stevens C. F. (1996) Cable properties of cultured hippocampal neurons determined from sucrose-evoked miniature EPSCs. *J. Neurophysiol.* **75,** 1250–1255.
2. Black J. A., Kocsis J. D. and Waxman S. G. (1990) Ion channel organization of the myelinated fiber. *Trends Neurosci.* **13,** 48–54.
3. Bliss T. and Collingridge G. L. (1993) A synaptic model of memory: Long-term potentiation in the hippocampus. *Nature* **361,** 31–39.
3a. Buzsáki G., Penttonen M., Nádasdy Z. and Bragin A. (1996) Pattern and inhibition-dependent invasion of pyramidal cell dendrites by fast spikes in the hippocampus *in vivo*. *Proc. natn. Acad. Sci. U.S.A.* **93,** 9921–9925.
4. Callaway J. C. and Ross W. N. (1995) Frequency-dependent propagation of sodium action potentials in dendrites of hippocampal CA1 pyramidal neurons. *J. Neurophysiol.* **74,** 1395–1403.
5. Cauller L. J. and Connors B. W. (1994) Synaptic physiology of horizontal afferents to layer I in slices of rat SI neocortex. *J. Neurosci.* **14,** 751–762.
5a. Colbert C. M. and Johnston D. (1996) Axonal action potential initiation and Na^+ channel densities in the soma and axon initial segment of subicular pyramidal neurons. *J. Neurosci.* **16,** 6676–6686.
6. Connors B. W., Gutnick M. J. and Prince D. A. (1982) Electrophysiological properties of neocortical neurons *in vitro*. *J. Neurophysiol.* **48,** 1302–1320.
6a. Contreras D., Destexhe A. and Steriade M. (1997) Intracellular and computational characterization of the intracortical inhibitory control of synchronized thalamic inputs *in vivo*. *J. Neurophysiol.* **78,** 335–350.
7. Coombs S. J., Curtis D. R. and Eccles J. C. (1957) The interpretation of spike potentials of motoneurons. *J. Physiol., Lond.* **139,** 198–231.
8. DeFelipe J. and Fariñas I. (1992) The pyramidal neuron of the cerebral cortex: morphological and chemical characteristics of the synaptic inputs. *Prog. Neurobiol.* **39,** 563–607.
9. Deschênes M. (1981) Dendritic spikes induced in fast pyramidal tract neurons by thalamic stimulation. *Expl Brain Res.* **43,** 304–308.
10. Destexhe A., Babloyantz A. and Sejnowski T. J. (1993) Ionic mechanisms for intrinsic slow oscillations in thalamic relay neurons. *Biophys. J.* **65,** 1538–1552.
11. Destexhe A., Mainen Z. F. and Sejnowski T. J. (1994) An efficient method for computing synaptic conductances based on a kinetic model of receptor binding. *Neural Comput.* **6,** 14–18.
12. Destexhe A., Mainen M. and Sejnowski T. J. (1997) Kinetic models of synaptic transmission. In *Methods in Neuronal Modeling* (eds Koch C. and Segev I.), 2nd edn. MIT Press, Cambridge, MA, (in press).
13. Douglas R. J., Martin K. A. and Whitteridge D. (1991) An intracellular analysis of the visual responses of neurones in cat visual cortex. *J. Physiol., Lond.* **440,** 659–696.
14. Fariñas I. and DeFelipe J. (1991) Patterns of synaptic input on corticocortical and corticothalamic cells in the visual cortex I. The cell body. *J. comp. Neurol.* **304,** 53–69.
15. Fariñas I. and DeFelipe J. (1991) Patterns of synaptic input on corticocortical and corticothalamic cells in the visual cortex. II The axon initial segment. *J. comp. Neurol.* **304,** 70–77.
16. Gähwiler B. H. and Brown D. A. (1985) $GABA_B$-receptor-activated K^+ current in voltage-clamped CA3 pyramidal cells in hippocampal cultures. *Proc. natn. Acad. Sci. U.S.A.* **82,** 1558–1562.
16a. Goldstein S. S. and Rall W. (1974) Changes in action potential shape and velocity for changing core conductor geometry. *Biophys. J.* **14,** 731–757.
17. Gutfreund Y., Yarom Y. and Segev I. (1995) Subthreshold oscillations and resonant frequency in guinea-pig cortical neurons—physiology and modeling. *J. Physiol., Lond.* **483,** 621–640.
18. Hamill O. P., Huguenard J. R. and Prince D. A. (1991) Patch-clamp studies of voltage-gated currents in identified neurons of the rat cerebral cortex. *Cerebr. Cortex* **1,** 48–61.
19. Hessler N. A., Shirke A. M. and Malinow R. (1993) The probability of transmitter release at a mammalian central synapse. *Nature* **366,** 569–572.
20. Hille B. (1992) *Ionic Channels of Excitable Membranes*. Sinauer, Sunderland, MA.
21. Hines M. (1993) NEURON: A program for simulation of nerve equations. In *Neural Systems: Analysis and Modeling* (ed. Eeckman F.), pp 127–136. Kluwer Academic Publishers, Boston, MA.
22. Hodgkin A. L. and Huxley A. F. (1952) A quantitative description of membrane currents to conduction and excitation in nerve. *J. Physiol., Lond.* **117,** 500–544.
23. Horikawa K. and Armstrong W. E. (1988) A versatile means of intracellular labeling: injection of biocytin and its detection with avidin conjugates. *J. Neurosci. Meth.* **25,** 1–11.
24. Huguenard J. R., Hamill O. P. and Prince D. A. (1988) Developmental changes in Na^+ conductances in rat neocortical neurons: appearance of a slowly inactivating component. *J. Neurophysiol.* **59,** 778–795.
25. Huguenard J. R., Hamill O. P. and Prince D. A. (1989) Sodium channels in dendrites of rat cortical pyramidal neurons. *Proc. natn. Acad. Sci. U.S.A.* **86,** 2473–2477.
25a. Jaffe D. B., Johnston D., Lasser-Ross N., Lisman J. E., Miyakawa H. and Ross W. N. (1992) The spread of sodium spikes determines the pattern of dendritic Ca entry into hippocampal neurons. *Nature* **357,** 244–246.
25b. Jahr C. E. and Stevens C. F. (1990) Voltage dependence of NMDA-activated macroscopic conductances predicted by single-channel kinetics. *J. Neurosci.* **10,** 3178–3182.
26. Johnston D. and Wu S. M. (1995) *Foundations of Cellular Neurophysiology*. Bradford Book/MIT Press, Cambridge, MA.
27. Johnston D., Magee J. C., Colbert C. M. and Christie B. R. (1996) Active properties of neuronal dendrites. *A. Rev. Neurosci.* **19,** 165–186.
28. Jones E. G. and Powell T. P. S. (1969) Morphological variations in the dendritic spines of the neocortex. *J. Cell Sci.* **5,** 509–529.

29. Jones E. G. and Powell T. P. S. (1970) Electron microscopy of the somatic sensory cortex of the cat. I. Cell types and synaptic organization. *Phil. Trans. R. Soc.* **257,** 1–11.
30. Kim H. G. and Connors B. W. (1993) Apical dendrites of the neocortex: Correlation between sodium- and calcium-dependent spiking and pyramidal cell morphology. *J. Neurosci.* **13,** 5301–5311.
31. Kim H. G., Beierlein M. and Connors B. W. (1995) Inhibitory control of excitable dendrites in neocortex. *J. Neurophysiol.* **74,** 1810–1814.
32. Larkman A. U. (1991) Dendritic morphology of pyramidal neurons of the visual cortex of the rat III. Spine distributions. *J. comp. Neurol.* **306,** 332–343.
32a. Llinás R. (1975) Electroresponsive properties of dendrites in central neurons. *Adv. Neurol.* **12,** 1–13.
33. Llinás R. and Hess R. (1976) Tetrodotoxin-resistant dendritic spikes in avian Purkinje cells. *Proc. natn. Acad. Sci. U.S.A.* **73,** 2520–2523.
34. Llinás R. and Nicholson C. (1971) Electrophysiological properties of dendrites and somata in alligator Purkinje cells. *J. Neurophysiol.* **34,** 532–551.
35. Llinás R. and Yarom Y. (1981) Electrophysiology of mammalian inferior olivary neurones *in vitro*. Different types of voltage-dependent ionic conductances. *J. Physiol., Lond.* **315,** 549–567.
36. Llinás R. and Yarom Y. (1981) Properties and distribution of ionic conductances generating electroresponsiveness of mammalian inferior olivary neurones *in vitro*. *J. Physiol., Lond.* **315,** 569–584.
37. Madison D. V. and Nicoll R. A. (1984) Control of the repetitive discharge of rat CA1 pyramidal neurones *in vitro*. *J. Physiol., Lond.* **354,** 319–331.
38. Magee J. C. and Johnston D. (1995) Characterization of single voltage-gated Na^+ and Ca^{2+} channels in apical dendrites of rat CA1 pyramidal neurons. *J. Physiol., Lond.* **487,** 67–90.
39. Magee J. C. and Johnston D. (1995) Synaptic activation of voltage-gated channels in the dendrites of hippocampal pyramidal neurons. *Science* **268,** 301–304.
40. Magee J. C., Christofi G., Miyakawa H., Christie B., Lasser R. N. and Johnston D. (1995) Subthreshold synaptic activation of voltage-gated Ca^{2+} channels mediates a localized Ca^{2+} influx into the dendrites of hippocampal pyramidal neurons. *J. Neurophysiol.* **74,** 1335–1342.
41. Mainen Z. F., Joerges J., Huguenard J. R. and Sejnowski T. J. (1995) A model of spike initiation in neocortical pyramidal neurons. *Neuron* **15,** 1427–1439.
42. Markram H. and Sakmann B. (1994) Calcium transients in dendrites of neocortical neurons evoked by single subthreshold excitatory postsynaptic potentials via low-voltage-activated calcium channels. *Proc. natn. Acad. Sci. U.S.A.* **91,** 5207–5211.
43. Mayer M. L. and Westbrook G. L. (1987) The physiology of excitatory amino acids in the vertabrate central nervous system. *Prog. Neurobiol.* **28,** 197–276.
44. McCormick D. A. and Prince D. A. (1986) Mechanisms of action of acetylcholine in the guinea-pig cerebral cortex *in vitro*. *J. Physiol., Lond.* **375,** 169–194.
45. McCormick D. A., Connors B. W., Lightall J. W. and Prince D. A. (1985) Comparative electrophysiology of pyramidal and sparsely spiny stellate neurons of the neocortex. *J. Neurophysiol.* **54,** 782–806.
45a. Migliore M. (1996) Modeling the attenuation and failure of action potentials in the dendrites of hippocampal neurons. *Biophys. J.* **71,** 2394–2403.
46. Mungai J. M. (1967) Dendritic patterns in the somatic sensory cortex of the cat. *J. Anat.* **101,** 403–418.
47. Otis T. S. and Mody I. (1992) Modulation of decay kinetics and frequency of GABA-A receptor-mediated spontaneous inhibitory postsynaptic currents in hippocampal neurons. *Neuroscience* **49,** 13–32.
47a. Peters A., Proskauer C. C. and Kaiserman-Abramof I. R. (1968) The small pyramidal neuron of the rat cerebral cortex: the axon hillock and the initial segment. *J. Cell Biol.* **39,** 604–619.
48. Peters A. and Kaiserman-Abramof I. R. (1970) The small pyramidal neuron of the rat cerebral cortex. The perikaryon, dendrites and spines. *Am. J. Anat.* **127,** 321–356.
49. Peters A., Palay S. L. and Webster H. F. (1981) *The Fine Structure of the Nervous System*. Oxford University Press, New York.
50. Press W. H., Flannery B. P., Teukolsky S. A. and Veterling W. T. (1986) *Numerical Recipes. The Art of Scientific Computing*. Cambridge University Press, Cambridge.
50a. Rall W. (1995) *The Theoretical Foundation of Dendritic Function*. MIT Press, Cambridge.
51. Rapp M., Yarom Y. and Segev I. (1996) Modeling back propagating action potentials in weakly excitable dendrites of neocortical pyramidal cells. *Proc. natn. Acad. Sci. U.S.A.* **93,** 11985–11990.
52. Regehr W. G., Kehoe J., Ascher P. and Armstrong C. (1993) Synaptically triggered action potentials in dendrites. *Neuron* **11,** 145–151.
53. Reuveni I., Friedman A., Amitai Y. and Gutnick M. J. (1993) Stepwise repolarization from Ca^{2+} plateaus in neocortical pyramidal cells: Evidence for nonhomogeneous distribution of HVA Ca^{2+} channels in dendrites. *J. Neurosci.* **13,** 4609–4621.
54. Schiller J., Helmchen F. and Sakmann B. (1995) Spatial profile of dendritic calcium transients evoked by action potentials in rat neocortical pyramidal neurones. *J. Physiol., Lond.* **487,** 583–600.
55. Schwindt P. C., Spain W. J., Foehring R. C., Stafstrom C. E., Chubb M. C. and Crill W. E. (1988) Multiple potassium conductances and their functions in neurons from cat sensorimotor cortex *in vitro*. *J. Neurophysiol.* **59,** 424–449.
56. Spruston N., Jaffe D. B., Williams S. H. and Johnston D. (1993) Voltage- and space-clamp errors associated with the measurement of electrotonically remote synaptic events. *J. Neurophysiol.* **70,** 781–802.
57. Spruston N., Jaffe D. B. and Johnston D. (1994) Dendritic attenuation of synaptic potentials and currents: the role of passive membrane properties. *Trends Neurosci.* **17,** 161–166.
58. Spruston N., Schiller Y., Stuart G. and Sakmann B. (1995) Activity-dependent action potential invasion and calcium influx into hippocampal CA1 dendrites. *Science* **268,** 297–300.
59. Stuart G. J. and Sakmann B. (1994) Active propagation of somatic action potentials into neocortical pyramidal cell dendrites. *Nature* **367,** 69–72.
59a. Svoboda K., Denk W., Kleinfeld D. and Tank D. W. (1997) *In vivo* dendritic calcium dynamics in neocortical pyramidal neurons. *Nature* **385,** 161–165.
60. Traub R. D. and Miles R. (1991) *Neuronal Networks of the Hippocampus*. Cambridge University Press, Cambridge.

61. Tsubokawa H. and Ross W. N. (1996) IPSPs modulate spike backpropagation and associated [Ca^{2+}] changes in the dendrites of hippocampal CA1 pyramidal neurons. *J. Neurophysiol.* **76,** 2896–2906.
62. White E. L. (1989) *Cortical Circuits*. Birkhauser, Boston, MA.
62a. Wollner D. A. and Catterall W. A. (1986) Localization of sodium channels in axon hillocks and initial segments of retinal ganglion cells. *Proc. natn. Acad. Sci. U.S.A.* **83,** 8424–8428.
63. Wong R. K. S., Prince D. A. and Basbaum A. I. (1979) Intradendritic recordings from hippocampal neurons. *Proc. natn. Acad. Sci. U.S.A.* **76,** 986–990.
64. Xiang Z., Greenwood A. C. and Brown T. (1992) Measurement and analysis of hippocampal mossy-fiber synapses. *Soc. Neurosci. Abstr.* **18,** 1350.
65. Yellen G. (1987) Permeation in potassium channels: implications for channel structure. *A. Rev. Biophys. biophys. Chem.* **16,** 227–246.
66. Yuste R. and Tank D. W. (1996) Dendritic integration in mammalian neurons, a century after Cajal. *Neuron* **16,** 701–716.
67. Yuste R., Gutnick M. J., Saar D., Delaney K. R. and Tank D. W. (1994) Ca^{2+} accumulations in dendrites of neocortical pyramidal neurons. *Neuron* **13,** 23–43.

(*Accepted* 7 *October* 1997)

APPENDIX

The multicompartment pyramidal neuron was described by conventional cable equations of a branched neuronal structure[50a] and solved using the NEURON simulator.[21] In each compartment, different types of ionic currents were inserted, including the leak current (I_L), the fast Na^+ current (I_{Na}), the "delayed-rectifier" K^+ current (I_{Kd}), a non-inactivating K^+ current (I_M) Additional currents were present in some simulations, such as the high-threshold Ca^{2+} current (I_{CaH}) and a Ca^{2+}-activated K^+ current ($I_{K[Ca]}$) Synaptic currents were simulated in all compartments and were I_{AMPA}, I_{NMDA} and I_{GABA_A}.

Intrinsic ionic currents

All active currents were expressed by the generic form

$$I_i = \bar{g}_i m^M h^N (V - E_i)$$

where $\bar{g}_i$ is the maximal conductance of current I_i and E_i is its reversal potential. The current activates according to M activation gates, represented by the gating variable m. It inactivates with N inactivation gates represented by the gating variable h. m and h obey to first-order kinetic equations.

The specific equations for each current are detailed below.

The Na^+ current I_{Na}[60]

$$I_{Na} = \bar{g}_{Na}\, m^3 h (V - E_{Na})$$

$$\frac{dm}{dt} = \alpha_m(V)\,(1-m) - \beta_m(V) m$$

$$\frac{dh}{dt} = \alpha_h(V)\,(1-h) - \beta_h(V) h$$

$$\alpha_m = \frac{-0.32(V - Tr - 13)}{\exp[-(V - Tr - 13)/4] - 1}$$

$$\beta_m = \frac{0.28(V - Tr - 40)}{\exp[(V - Tr - 40)/5] - 1}$$

$$\alpha_h = 0.128 \exp[-(V - Tr - 17)/18]$$

$$\beta_h = \frac{4}{1 + \exp[-(V - Tr - 40)/5]}$$

where $Tr = -63$ mV.

The delayed-rectifier K^+ current I_{Kd}[60]

$$I_{Kd} = \bar{g}_{Kd}\, n^4 (V - E_K)$$

$$\frac{dn}{dt} = \alpha_n(V)(1-n) - \beta_n(V)\, n$$

$$a_n = \frac{-0.032(V - Tr - 15)}{\exp[-(V - Tr - 15)/5] - 1}$$

$$\beta_n = 0.5 \exp[-(V - Tr - 10)/40]$$

The non-inactivating K^+ current I_M[17]

$$I_M = \bar{g}_M \, n(V - E_K)$$

$$\frac{dn}{dt} = a_n(V)(1 - n) - \beta_n(V) \, n$$

$$a_n = \frac{0.0001(V + 30)}{1 - \exp[-(V + 30)/9]}$$

$$\beta_n = \frac{-0.0001(V + 30)}{1 - \exp[(V + 30)/9]}$$

The high-threshold Ca^{2+} current I_{CaH}[53]

$$I_{CaH} = \bar{g}_{CaH} m^2 h(V - E_{Ca})$$

$$\frac{dm}{dt} = a_m(V)(1 - m) - \beta_m(V) \, m$$

$$\frac{dh}{dt} = a_h(V)(1 - h) - \beta_h(V) \, h$$

$$a_m = \frac{-0.055(V + 27)}{\exp[-(V + 27)/3.8] - 1}$$

$$\beta_m = 0.94 \exp[-(V + 75)/17]$$

$$a_h = 0.000457 \exp[-(V + 13)/50]$$

$$\beta_h = \frac{0.0065}{1 + \exp[-(V + 15)/28]}$$

The Ca^{2+}-activated K^+ current $I_{K[Ca]}$

$$I_{K[Ca]} = \bar{g}_{K[Ca]} n^2(V - E_k)$$

$$\frac{dn}{dt} = a_n [Ca]_i^2 \, (1 - n) - \beta_n n$$

where $[Ca]_i$ is the intracellular calcium concentration, $\alpha_n = 2000 \text{ mM}^{-2}\text{ms}^{-1}$ and $\beta_n = 0.002 \text{ ms}^{-1}$. The dynamics of intracellular calcium in a thin shell of $d = 0.1$ μm beneath the membrane was given by:

$$\frac{d[Ca]_i}{dt} = -\frac{1}{2Fd} I_{CaH} - ([Ca]_i - Ca_\infty)/\tau_{Ca}$$

Here, the first term represents the influx of Ca^{2+} ions due to Ca^{2+} currents and the second term represents the efflux of Ca^{2+} due to active clearance and buffering ($Ca_\infty = 240$ nM and $\tau_{Ca} = 5$ ms; see details in Ref. 10).

The reversal potential for Ca^{2+} was given by the Nernst relation:

$$E_{Ca} = \frac{RT}{2F} \log \frac{[Ca]_o}{[Ca]_i}$$

where $R = 8.31$ J mol^{-1} K^{-1}, $T = 309$ K, and the extracellular calcium concentration was $[Ca]_o = 2$ mM. For $[Ca]_i = 240$ nM, which is the resting value in the simulations presented here, E_{Ca} was approximately 120 mV.

Synaptic currents

Synaptic currents were described by the generic equation:

$$I_j = \bar{g}_j \, m(V - E_j)$$

where $\bar{g}_j$ is the maximal conductance of postsynaptic receptors and E_j is the reversal potential. m is the fraction of open receptors according to the simple first-order kinetic equation:[11]

$$\frac{dm}{dt} = \alpha \, T(1 - m) - \beta \, m$$

where T is the concentration of transmitter in the cleft. Synaptic activation was simulated by setting T to 1 mM during 1 ms, leading to the transient activation of the current. Receptor types such as AMPA, NMDA and $GABA_A$ were described by such a scheme for the activation variable m. Based on whole-cell recordings of hippocampal pyramidal and dentate gyrus neurons,[19,47,64] the kinetic parameters of these models for $GABA_A$, NMDA and AMPA receptors were obtained by fitting the model to experimental data using a simplex procedure (see details in Ref. 12).

The specific equations for the current mediated by each type of receptor are given below (see Ref. 12 for more details).

AMPA receptors

$$I_{AMPA} = \bar{g}_{AMPA} m(V - E_{AMPA})$$

where $E_{AMPA} = 0$ mV, $\alpha = 1.1 \times 10^6 \, M^{-1}s^{-1}$ and $\beta = 180 \, s^{-1}$.

$GABA_A$ receptors

$$I_{GABA_A} = \bar{g}_{GABA_A} m(V - E_{Cl})$$

where $E_{Cl} = -80$ mV, $\alpha = 5 \times 10^6 \, M^{-1}s^{-1}$ and $\beta = 180 \, s^{-1}$.

NMDA receptors

The activation of NMDA receptors contained an additional voltage-dependent term due to magnesium-block:[25b]

$$I_{NMDA} = \bar{g}_{NMDA} m \, B(V)(V - E_{NMDA})$$

$$B(V) = \frac{1}{1 + \exp(-0.062V)[Mg]_o / 3.57}$$

where $[Mg]_o = 2$ mM is the extracellular magnesium concentration, $E_{NMDA} = 0$ mV, $\alpha = 7.2 \times 10^4 \, M^{-1}s^{-1}$ and $\beta = 6.6 \, s^{-1}$.